ISSN 0915-6364

NATIONAL INSTITUTE FOR FUSION SCIENCE

Dielectronic Recombination of Xe^{10+} Ions and Satellite line of Xe^{9+} Ions

M.-Y. Song and T. Kato

(Received - Aug. 26, 2005)

NIFS-DATA-94 Oct. 2005

RESEARCH REPORT
NIFS-DATA Series

TOKI, JAPAN

Dielectronic Recombination of Xe^{10+} Ions and Satellite Line of Xe^{9+} Ions

M.-Y. Song and T. Kato

National Institute for Fusion Science

EUV light sources from compact plasmas are now intensively studied for the next generation of lithography. The multicharged Xe ions emit EUV emission and are now investigated extensively. However we do not know the detailed atomic processes for the Xe ions. We study in this paper on dielectronic and radiative recombination processes of Xe ions. We have calculated the energy levels, radiative transition probabilities (Ar), autoionization rates (Aa), and radiative recombination cross section for Xe^{10+} ions using the FAC code. The dielectronic recombination rate coefficient(α_{DR}) from the Xe^{10+} ions and the related dielectronic satellite lines are obtained. We studied the n- and l-dependence for Ar, Aa, dielectronic recombination rate coefficient(α_{DR}), and radiative recombination rate coefficient(K_{rr}). The dielectronic recombination processes from the $4d^8 + e \rightarrow 4d^7 4f^1 nl \rightarrow 4d^8 nl + h\nu$ and the $4d^8 + e \rightarrow 4d^7 5p^1 nl \rightarrow 4d^8 nl + h\nu$ become important at low plasma temperature $Te \approx 10eV$ for line intensities. Also, the radiative recombination rate coefficient is smaller than the values of the dielectronic recombination processes in our interested temperature region at Te = 1eV - 1000eV.

Keyword: Dielectronic recombination, Satellite line, Xe^{10+}, Radiative recombination

1. Introduction

Dielectronic recombination(DR)[1-5] is the dominant electron-ion recombination process for low charged ions in high-temperature and low density plasmas. Therefore, it is very important in determining the ionization balance. Another very important role of dielectronic recombination is connected with the presence of so-called satellite lines produced through the radiative decay of autoionzing states. Such spectral lines give information not only about ion structure but also about plasma parameters i.e., plasma density and plasma temperature, and therefore, played an essential role in X-ray spectroscopy and plasma diagnostics. The dielectronic recombination is a resonant, two step processes in which a multicharged ion X_Z captures a free electron with simultaneous excitation of the target electron and creates a doubly excited ion X_{Z-1}, which then decays by a radiative transition.

$$X_Z(i_0) + e \rightarrow X_{Z-1}^{**}(i) \rightarrow X_{Z-1}^{*}(f) + h\nu \tag{1}$$

where X_{Z-1}^{**} expresses the autoionization state of the X_{Z-1} ion and i_0, i, and f denote the sets of quantum states of an ion in the initial state(i_0), doubly excited target electron state(i) , and final state(f). Another competitive process for the decay of an ion X_{Z-1}^{**} is the autoionization process. As the interest about Xenon ions grows recently for EUV sources, many people are working on the research about Xenon ions. We need data about atomic collisional processes of Xenon ion to analyze Xenon spectra. However, as long as we know, there are few papers which give us enough data of the dielectronic recombination rate coefficient to each final bound state. These data are necessary to estimate the population of the excited states by a collisional radiative model. In this report, we calculated the data for the dielectronic recombination from Xe^{10+} ions to the excited states of Xe^{9+} ions. We investigate the $4d^7 5p^1 nl$ and $4d^7 4f^1 nl$ states as autoionizing states, which are important for the dielectronic recombination process. We use the Flexible Atomic Code (FAC)[6-8] for calculating the atomic data for dielectronic recombination rate coefficient. In section 2, we describe the atomic data about the energy levels, the radiative transition probabilities, and the autoionization rates. In section 3, we calculate the DR rate coefficient to the excited states and the total DR rate coefficients. In section 4, we obtain the dielectronic satellite lines through the radiative transitions of $4d^7 5p^1 nl - 4d^8 nl$ and $4d^7 4f^1 nl - 4d^8 nl$. In section 5, we calculate the total radiative recombination rate coefficient of Xe^{10+} ions. Finally, in section 6, we summarize our results.

2. Atomic data using Flexible Atomic Code (FAC)

The atomic structure calculation in the FAC[6-8] made by M. F. Gu is based on the relativistic configuration interaction with independent particle basis wavefunctions. These basis wavefunctions are derived from a local central potential, which is self-consistently determined to represent electronic screening of the nuclear potential. The bound states of the atomic system are calculated in the configuration mixing approximation with convenient specification of mixing schemes. The radial orbitals for the construction of basis states are derived from a modified self-consistent Dirac-Fock Slater interaction on a fictitious mean configuration with fractional occupation numbers, representing the average electron cloud of the configurations included in the calculation. The radiative transition rates are calculated in a single multipole approximation with arbitrary ranks. This means that the interference between different multipoles is not taken into account, although rates corresponding to arbitrary multipoles can be calculated. For a given multipole operator O^L_M, and initial and final states of the transition $\psi_i = \sum_\nu b_{i\nu}\Phi_\nu$ and $\psi_f = \sum_\mu b_{f\mu}\Phi_\mu$, the line strength of the transition is

$$S_{fi} = | < \psi_f | O^L_M | \psi_i > |^2. \tag{2}$$

The weighted oscillator strength and transition rates are given by

$$g_f f_{fi} = [L]^{-1}\omega(\alpha\omega)^{2L-2}S_{fi}, \tag{3}$$

$$g_f A_{fi} = 2\alpha^3\omega^2 g_f f_{fi}, \tag{4}$$

where $[L] = 2L+1$, L is the total orbital angular momentum, $\omega = E_i - E_f$ is the transition energy and α is the fine structure constants. The calculation of the autoionization rates is based on the distorted-wave(DW) approximation. The method implements an efficient interpolation procedure for the calculation of the autoionzation radial integral. The calculation of autoionization rates is the major task in any distorted-wave treatments of resonant processes. The present method to calculate the autoionizing rate is similar to that of Oreg et al.[9], which uses an efficient factorization-interpolation procedure for the calculation of the autoionization radial integrals. The autoionization transition rate can be written as

$$Aa = 2\sum_k \left| < \psi_f, \kappa; J_T M_T | \sum_{i<j} \frac{1}{r_{ij}} |\psi_i > \right|^2 \tag{5}$$

where ψ_i is the autoionizing state, ψ_f is the final state which has one less electron than ψ_i, κ is the relativistic angular quantum number of the free electron. The total angular momentum of the coupled final state must be equal to that of ψ_i, i.e., $J_T = J_i$ and $M_T = M_i$. Also, the partial photoionization (PI) cross section can be expressed in terms of the differential oscillator strength(in atomic unit), and the partial radiative recombination (RR) cross section is related to the PI through the Milne relation

$$\sigma_{PI} = 2\pi\alpha\frac{1+\alpha^2\epsilon}{1+0.5\alpha^2\epsilon}\frac{df}{dE} \tag{6}$$

$$\sigma_{RR} = \frac{\alpha^2}{2}\frac{g_i}{g_f}\frac{\omega^2}{\epsilon(1+0.5\alpha^2\epsilon)}\sigma_{PI} \tag{7}$$

where α is the fine structure constant, g_i and g_f are the statistical weights of the bound states before and after the photoionization takes place respectively, ω is the photon energy, and ϵ is the energy of the ejected photo-electron. The differential oscillator strength, df/dE, may be calculated similarly to the bound-bound oscillator strength through the generalized line strength

$$\frac{df}{dE} = \frac{\omega}{g_i}[L]^{-1}(\alpha\omega)^{2L-2}S, \tag{8}$$

where L is the rank of the multipole operator inducing the transition, $[L]$ denotes $2L+1$, and the generalized line strength is

$$S = \sum_{\kappa J_T} |< \psi_f, \kappa; J_T \parallel O^L \parallel \psi_i >|^2, \tag{9}$$

where κ is the relativistic quantum number of the free electron, J_T is the total angular momentum of the free state when the final bound state is coupled to the continuum electron, and O^L is the multipole operator inducing the transition.

Table 1 shows all the final energy levels of the $4p^6 4d^8$ configuration of Xe^{10+} ions from the levels of the $4p^6 4d^9$ configuration of Xe^{9+} ion which we calculated using the FAC code. Numbers marked in the first column of the table will be used to identify different energy levels. Figures 1 and 2 show the energy levels of the ground and excited states of Xe^{10+} and of the autoionizing and excited states of Xe^{9+}. Figure 1 shows the levels for the transitions $4d-4f$ whereas figure 2 shows the levels for transitions for $4d-5p$. Through these figures, we know that the levels of $4d^7 4f^2, 4d^7 4f^1 5l$, and $4d^7 5p^1 5d^1 (5f^1, 5g^1)$ are crossing the ionization limit of Xe^{9+}. Some of the levels are autoionizing states which are above the ionization limit of Xe^{9+} and other levels are below the ionization limit. Tables 2 and 3 show the comparison of the averaged radiative transition $(4d^8 nl - 4d^7 5p^1 n'l')$ rates ($\bar{A}r \equiv \frac{\sum_{i,j} g_i Ar_{ij}}{\sum_i g_i}$) and autoionization rates ($\bar{A}a \equiv \frac{\sum_{i,j} g_i Aa_{ij}}{\sum_i g_i}$) calculated with the HULLAC[10] and the FAC program. Through above result, we can know that two calculations show similar result.

3. Dielectronic recombination rate coefficients for Xe^{10+}

The Dielectronic recombination (DR) rate coefficients, $\alpha_{DR}(i_0, f; T_e)$, for electrons in the Maxwellian distribution can be expressed as

$$\alpha_{DR}(i_0, i, f; T_e) = \left(\frac{h^3}{2\pi m_e k_B T_e}\right)^{3/2} \frac{1}{2g_{i_0}} Qd(i_0, i, f) e^{(\frac{-E_{i,i_0}}{k_B T_e})}, \tag{10}$$

where T_e is the electron temperature, m_e is the electron mass, h is the Plank constant, k_B is the Boltzmann constant, g_i and g_{i_0} are the statistical weights of the autoionizing state (i) formed by dielectronic capture and the target state (i_0) before dielectronic capture, and E_{i,i_0} is the resonance energy calculated from the ionization limit. This schematic diagram for DR is shown in Fig I.

The intensity factor (Qd) for the dielectronic satellite lines from i to f are given by

$$Qd(i_0, i, f) = \frac{g_i Aa(i, i_0) Ar(i \to f)}{\sum_{all\ i_0'} Aa(i, i_0') + \sum_{all\ f'} Ar(i \to f')}. \tag{11}$$

where g_i and g_0 are the statistical weights of the intermediate(autoionization) state i and initial state i_0 of Xe^{10+}, $Ar(i \to f)$ is the radiative decay rate from the level i to the level f, $Aa(i, i_0)$ is the autoionization rate from the level i to the level i_0. The sum over i_0' runs over all the levels in the next higher ion reachable from the level i by autoionization, and the sum over f' runs over all bound levels reachable from the level i by radiative decay.

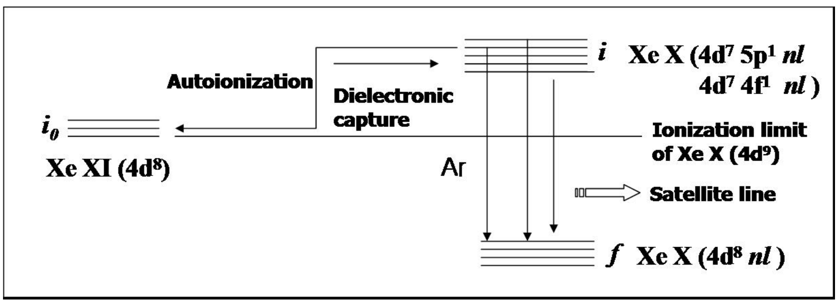

Figure I. Dielectronic recombination process

The autoionizing states formed by dielectronic capture may either autoionize, or radiatively decay. The radiative decay to the states below the ionization limit completes the recombination process. The radiative branching ratio for dielectronic recombination can be expressed as $\frac{Ar(i\rightarrow f)}{\sum Aa+\sum Ar}$. Usually, the states of each complex, designated as $n'l'nl$, where the excited core electron $(n'l')$ and the capture electron (nl) have the principle quantum numbers, $\Delta n' = 0$ and $\Delta n' = 1$ are considered separately. The $\Delta n' = 0$ resonances, where the transition of the core electron does not change its principle quantum number, and $\Delta n' = 1$ resonances, where the principle quantum number of the core electron changes by one unit, make dominant contributions to the total DR rate coefficients at temperatures of interest. Figure 3-(a) shows the average $\bar{A}r[\equiv \Sigma g_i A_{ij}/\Sigma g_i]$ values of the $4d^7 4f^1 nd \rightarrow 4d^8 nd$ and $4d^7 5p^1 nd \rightarrow 4d^8 nd$ as a function of the principle quantum number n at $l = 2$. Figure 3-(b) shows the average $\bar{A}a[\equiv \Sigma g_i Aa_{i,i_0}/\Sigma g_i]$ values of the $4d^7 4f^1 nd \rightarrow 4d^8 + e$ and $4d^7 5p^1 nd \rightarrow 4d^8 + e$ as a function of the principle quantum number n at $l = 2$. Figure 4-(a) shows the average $\bar{A}r$ of transition of $4d^7 4f^1 7l \rightarrow 4d^8 7l$ and $4d^7 5p^1 7l \rightarrow 4d^8 7l$ as a function of the angular quantum number l and figure 4-(b) shows the average $\bar{A}a$ of transition of $4d^7 4f^1 7l \rightarrow 4d^8 + e$ and $4d^7 5p^1 7l \rightarrow 4d^8 + e$ as a function of the angular quantum number l. The average $\bar{A}r$ keeps almost constant with increasing l but the average $\bar{A}a$ is decreased with increasing l, except $l = 3$. The summation over nl, however, can potentially involve large number of terms. For high n, the contributions for large l are small. For estimating contributions from autoionizaing states with higher n levels for $n > 15$, we use empirical scaling laws.

$$Ar(4d^7 4f^1 nl \rightarrow 4d^8 nl) \simeq Ar(4d^7 4f^1 15l \rightarrow 4d^8 15l), \tag{12}$$

$$Ar(4d^7 5p^1 nl \rightarrow 4d^8 nl) \simeq Ar(4d^7 5p^1 15l \rightarrow 4d^8 15l), \tag{13}$$

$$Aa(4d^7 4f^1 nl, 4d^8) \simeq Aa(4d^7 4f^1 15l, 4d^8)\left(\frac{15}{n}\right)^3, \tag{14}$$

$$Aa(4d^7 5p^1 nl, 4d^8) \simeq Aa(4d^7 5p^1 15l, 4d^8)\left(\frac{15}{n}\right)^3. \tag{15}$$

We extrapolate Ar and Aa values from $n = 15$ for the scaling. When we calculate the dielectronic recombination rate coefficients, we calculate the data of $n \leq 15$ and $l \leq n-1$ by the FAC code. In order to obtain the DR rate coefficient, we assumed the population density of the ground state $4d^8(i_0)$ is proportional to the statistical weight.

$$\begin{aligned}\alpha_{DR}(i,f) &\equiv \frac{1}{2}\Big(\frac{h^3}{2\pi m_e k_B T_e}\Big)^{3/2} \frac{\sum_{i_0} g_0 Qd(i_0,i,f)/g_0}{\sum_{i_0} g_0} \times e^{-(\frac{\Delta E_s}{k_B T_e})} \\ &= \frac{1}{2}\Big(\frac{h^3}{2\pi m_e k_B T_e}\Big)^{3/2} < Qd(i_0,i,f)/g_0 > e^{-(\frac{\Delta E_s}{k_B T_e})} \qquad (16)\end{aligned}$$

Figures 5 and 6 show the dielectronic recombination rate coefficients for the $4d^8 + e \rightarrow 4d^7 4f^1 nd \rightarrow 4d^8 nd + h\nu$ and $4d^8 + e \rightarrow 4d^7 5p^1 nd \rightarrow 4d^8 nd + h\nu$, respectively, for different values n with a fixed l value as a function of electron temperature. The maximum position of the dielectronic recombination rate coefficients moves towards high temperature region with increasing n for $n < 10$, whereas, the maximum position of the dielectronic recombination rate coefficients does not change with increasing n for $n > 10$. Figures 7 and 8 show the temperature dependence of the dielectronic recombination rate coefficient calculated for different l with a fixed $n = 7$. The value of the dielectronic recombination rate coefficients for the $4d^8 + e \rightarrow 4d^7 4f^1 7l \rightarrow 4d^8 7l + h\nu$ and $4d^8 + e \rightarrow 4d^7 5p^1 7l \rightarrow 4d^8 7l + h\nu$ increase with increasing l and reach the maximum at $l = 5$. This is because Aa values decrease rapidly and are comparable to Ar values for $l > 5$ as shown in figure 4. Also, the maximum position of these values moves towards high temperature region with increasing l. Figures 9 and 10 show the dielectronic recombination rate coefficients summed over all l but for each different n as a function of the electron temperature. The maximum values of the dielectronic recombination rate coefficients for the $4d^8 \rightarrow 4d^7 4f^1 nl \rightarrow 4d^8 nl$ and $4d^8 \rightarrow 4d^7 5p^1 nl \rightarrow 4d^8 nl$ moves from 10eV to 50eV for high n. The difference of the values between n and $n+1$ of the dielectronic recombination rate coefficient for the $4d^8 \rightarrow 4d^7 4f^1 nl \rightarrow 4d^8 nl$ and $4d^8 \rightarrow 4d^7 5p^1 nl \rightarrow 4d^8 nl$ decreases as n value increases as shown in figures 9 and 10. We can see that the results of the dielectronic recombination rate coefficients for the $4d^8 + e \rightarrow 4d^7 4f^1 nl \rightarrow 4d^8 nl + h\nu$ and $4d^8 + e \rightarrow 4d^7 5p^1 nl \rightarrow 4d^8 nl + h\nu$ at $n = 4$ and 5 are different from other levels, because the values of E_{i,i_0} of $4d^7 4f^1 nl$ and $4d^7 5p^1 nl$ at $n = 4$ and 5 are much smaller than other. The DR rate coefficient for $n = 4$ and 5 are large at low temperatures as shown in figures 9 and 10. The total dielectronic recombination rate coefficient is given by

$$\alpha_{DR}^{tot}(T_e) \quad = \quad \frac{1}{2}\Big(\frac{h^3}{2\pi m_e k_B T_e}\Big)^{3/2} \sum_{i,f} < Qd(i_0, i, f)/g_0 > e^{-(\frac{\Delta E_s}{k_B T_e})} \qquad (17)$$

where g_i and g_0 are the statistical weights of the intermediate(autoionization) state i of Xe^{9+} and initial states i_0 of Xe^{10+}, ΔE_s and $< Qd(i_0)/g_0 >$ represent the average value over all initial state the Xe^{10+}(4d^8). Figure 11 shows the total dielectronic recombination rate coefficient calculated for the following $4d^8 \rightarrow 4d^7 4f^1 nl \rightarrow 4d^8 nl$ and $4d^8 \rightarrow 4d^7 5p^1 nl \rightarrow 4d^8 nl$ processes. The number I and II represent the transition of $4d^8 \rightarrow 4d^7 4f^1 nl \rightarrow 4d^8 nl$ and $4d^8 \rightarrow 4d^7 5p^1 nl \rightarrow 4d^8 nl$, respectively, including $n = 4 - 100$, $l = n - 1$ for $n \leq 15$, and $l = 0 - 6$ for $n > 15$. The I' and II' represent the transitions including $n = 1 - 15$ and $l = n - 1$. The total dielectronic recombination rate coefficients have the maximum values at around 50eV and the temperatures at maximum values increase towards higher electron temperature with larger n and l.

4. Satellite lines of Xe^{10+}

The satellite lines [5,11,12] for Xe^{10+} parent emission of the types $4d^8 - 4d^7 4f^1$ and $4d^8 - 4d^7 5p^1$ transitions are emitted by the radiative stabilization from the doubly excited states in the Xe^{9+} ions: $4d^7 4f^1 nl - 4d^8 nl$ and $4d^7 5p^1 nl - 4d^8 nl$. During the stabilization, the additional nl electron (a nonparticipating, so-called spectator electron) perturbs the other orbitals by shielding the nuclear charge resulting in a transition wavelength somewhat longer than that of the parent transition. These satellite lines are of great interest in fields of study involving laboratory, astrophysics and particularly in diagnostics of plasmas, where they are used to determine the electron temperature or electron density through intensity ratios. The doubly excited states are populated by the processes of dielectronic capture:

$$e^- + Xe^{10+}(4d^8) \longrightarrow Xe^{9+}(4d^7 4f^1 nl) \longrightarrow Xe^{9+}(4d^8 nl) + h\nu, \tag{18}$$

$$e^- + Xe^{10+}(4d^8) \longrightarrow Xe^{9+}(4d^7 5p^1 nl) \longrightarrow Xe^{9+}(4d^8 nl) + h\nu \tag{19}$$

The dielectronic recombination process is resonated by the incident electron energy, required being equal to the energy of the doubly excited state relative to the ionization energy of the Xe^{9+} ion. The autoionization takes place only when the energy of the doubly excited states is above the threshold energy. The ionization energy from the ground state $4p^6 4d^9$ of Xe^{9+} ion is about 1,627,000 cm^{-1} (201.7 eV)[13]. The emissivity of a dielectronic satellite transition from the autoionizing state i to a final state f is proportional to a $Qd(i_0, i, f)$ factor which expresses the rate of dielectronic capture into the autoionizing state followed by radiative decay to the final state. Thus, the intensity of a satellite lines produced by dielectronic recombination can be expressed by Eq. (10). Tables 4 - 6 show the wavelength(λ) , radiative transition probability(Ar), autoionization rate(Aa), energy difference(δE_i) between the autoionization state(i) and the initial state(i_0), and the intensity factor(Qd) for the transitions from the $4d^8(i_0) \rightarrow 4d^7 4f^2(i) \rightarrow 4d^8 4f^1(f)$ at $i_0 = 0, 4$, and 6 of the Xe^{10+} ions which capture the free electron. Tables 7 - 9 show the wavelength(λ) , radiative transition probability(Ar), autoionization rate(Aa), energy difference(δE_i) between the autoionization state(i) and the initial state(i_0), and the intensity factor(Qd) for the transitions from the $4d^8(i_0) \rightarrow 4d^7 5p^1 5d^1(i) \rightarrow 4d^8 4f^1(f)$ at $i_0 = 0, 4$, and 6 of the Xe^{10+} ions which capture the free electron. Here the g_f is statistical weight of the each final excited state of the Xe^{9+} and the g_i is statistical weight of the autoionization state of the Xe^{9+}. We select the strong satellite lines which have the values Qd larger than 10^{10}. When the satellite line of Xe^{9+} are observed, the satellite line appear near the parent emission of Xe^{10+}. The parent emission lines are generally produced by an excitation process. It is necessary to know the contribution of satellite lines on the excitation lines. We calculated the excitation rate coefficient from level i to level i' ($C_{i,i'}$) using the FAC code. Figures 12 and 13 show the collisional excitation rate coefficients for the $4d^8(2J = 8) \to 4d^7 4f^1$(2J=8) (111.572$\dot{A}$) and $4d^8(2J = 8) \to 4^7 5p^1$(2J=10) (135.859$\dot{A}$) of Xe^{10+} ions and the dielectronic recombination rate coefficients for the $4d^8(2J = 8) \to 4d^7 4f^2(2J = 15) \to 4d^8 4f^1(2J = 13)$ (112.3256$\dot{A}$) and $4d^8 \to 4d^7 5p^1 5d^1(2J = 11) \to 4d^8 5d^1(2J = 13)$ (136.0335$\dot{A}$) as a function of electron temperature for the lines which intensities are the largest. Through these results, we can expect that the satellite line intensity is larger than the excitation intensity at low temperature ($Te < 10$eV). Here we assumed the line intensity by excitation is proportional to the excitation from the ground state.

$$I_{parent}(i', i_0) \quad = \quad C_{i_0,i'} n_z n_e, \tag{20}$$

Figures 14(a)- 16(a) show the intensity factor(Qd) of the satellite transitions from $4d^7 4f^2$ to $4d^8 4f^1$ for the initial configuration ($4d^8$) with different J-values ($i_0 = 0, 4, 6$) of the Xe^{10+} ions. Figures 14(b) -16(b) show the intensity factor (gAr) for lines emitted from the excited state $4d^7 4f^1$ to the ground state $4d^8$ of the Xe^{10+} ions ($i_0 = 0, 4, 6$). For these lines, the population densities of the excited states are assumed proportional to the statistical weights g of the excited states. Here the intensity factors are convoluted by the Gaussian profiles with spectral Doppler width $\Delta\sigma = 0.0138\dot{A}$. It is shown that the spectra are quite different when the initial state J is different. Figures (a) and (b) of the figures 17 to 19 compare the intensity factor(Qd) of the satellite transitions from the states of $4d^7 5p^1 5d^1$ to $4d^8 5d^1$ for the different initial states $4d^8$ ($i_0 = 0, 4, 6$) of the Xe^{10+} ions and the intensity factor(gAr) for the lines emitted from the excited state $4d^7 5p^1$to the ground state $4d^8$ of the Xe^{10+} ions ($i_0 = 0, 4, 6$).

We compare the spectral shape of excitation lines and satellite lines for the intensity averaged over the initial ground states ($4d^8$) given in Table 1. The population densities of the ground states are assumed to be proportional to the statistical weights. In the case of satellite lines, the DR rate coefficient is the same as the intensity of the satellite lines from the dielectronic recombination process. Thus the intensity of the satellite lines from the dielectronic recombination process is given by

$$I_{satellite}(i,f) \;=\; \frac{1}{2}\Big(\frac{h^3}{2\pi m_e k_B T_e}\Big)^{3/2} e^{-(\frac{\Delta E_s}{k_B T_e})} < Qd(i_0,i,f)/g_0 > n_z n_e, \qquad (21)$$

where g_i and g_0 are the statistical weights of the intermediate(autoionization) state i of Xe^{9+} and initial states i_0 of Xe^{10+}, ΔE_s and $< Qd(i_0)/g_0 >$ represent the average values over all initial state of the $\mathrm{Xe}^{10+}(\mathrm{4d}^8)$. In the case of lines produced by direct excitation, the excitation rate coefficient contributes to the intensity of lines. For the line intensities by excitation, we assumed that the population densities of the excited states are proportional to the statistical weights: $I_{parent}(i',i_0) \propto g_i' A_{i',i_0}$. Figures 20(a) and 20(b) compare the average intensity factor ($< Qd(4d^7 4f^2, 4d^8 4f^1)/g_0 >$ for the satellite transitions from the states of $4d^7 4f^2$ to $4d^8 4f^1$ after the initial states ($4d^8$) of the Xe^{10+} ions captures the free electron and the intensity factor($g_{i'} Ar(4d^8, 4d^7 4f^1)$) for the lines from $4d^7 4f^1$ to $4d^8$ of the Xe^{10+} ions. Also, figures 21(a) and 21(b) compare the average intensity factor ($< Qd(4d^7 5p^1 5d^1, 4d^8 5d^1)/g_0 >$) for the satellite transitions from the states of $4d^7 5p^1 5d^1$ to $4d^8 5d^1$ and the intensity factor($g_{i'} Ar(4d^8, 4d^7 5p^1)$) for the lines from $4d^7 5p^1$ to $4d^8$ of the Xe^{10+} ions. When we observe the satellite lines, the lines for the transitions $4d^7 4f^1 nl - 4d^8 nl$ and $4d^7 5p^1 nl - 4d^8 nl$ including $n > 4$ are observed. We calculated the spectra summing up to $n = 7$ for $\sum_{n=4}^{7} < Qd(4d^8, 4d^7 4f^1 nl, 4d^8 nl)/g_0 >$ and $\sum_{n=5}^{7} < Qd(4d^8, 4d^7 5p^1 nl, 4d^8 nl)/g_0 >$. They are shown in figures 22 and 23. Comparing to the values shown in Figs. 20 and 22 or Figs. 21 and 23 , we can know the contribution of high n are important for the satellite line. We know that the dielectronic satellite lines of Xe^{9+}

ions appear near the excitation lines of Xe^{10+} ions and the dielectronic satellite lines have values of intensities that can not be ignored at low temperate. For identification of the spectrum from the highly charged ions, we need the information of the direct excitation of the parent ions.

5. Radiative recombination processes

In radiative recombination, a free electron is directly captured by a target, releasing its kinetic energy and binding energy of the final bound state to the emitted photon. Radiative recombination is an important contributor to the total recombination rate coefficient at least in some temperature ranges. When we consider the recombination processes, it is necessary to know the contribution of radiative recombination.

$$e^- + Xe^{10+}(4d^8) \longrightarrow Xe^{9+}(4d^8nl) + h\nu \tag{22}$$

Generally, the radiative recombination (RR) cross section is obtained from the photoionization (PI) cross sections through the Milne relation. The PI cross section for the $n \leq 10$ shells are calculated in the distorted-wave approximation, taking into account the electronic dipole operator. The wave functions of bound and continuum orbitals are obtained by solving the single-electron Dirac equations with a spherical model potential, which is based on the self-consistent Dirac-Fork-Slater calculation. The atomic code for our calculation is the FAC code. The PI cross sections is computed at electron energies of $E_e < 10E_{th}$, where the E_{th} values are the ionization thresholds for corresponding shells. For $E_e > 10E_{th}$, the FAC code used a simplified version of the formula suggested by Verner et al.[14] until 10000eV ,

$$\sigma_{PI}(E_e) = \sigma_0 x^{-3.5-1+p/2}\Big(\frac{1+b}{\sqrt{x}+b}\Big)^p \tag{23}$$

where $x = (E_0 + E_e)/E_0$, l is the orbital angular momentum of the photoionized shell, and σ_0, E_0, p, and b are fit parameters. For the photoionization of a particular nl shell, we calculate the exact nonrelativistic cross sections of the hydrogenic ion with the residual nuclear charge and fit them with the above equation, fixing E_0 to be the binding energy of the orbital. Therefore, the FAC code includes these two kind of calculations, which are the exact calculation at $E_e < 10E_{th}$ and fit formula at $E_e > 10E_{th}$. We obtained the radiative recombination to the excited state nl from the the photoionization of a particular nl shell.

The radiative recombination cross section obtained from the FAC code is fitted by series of terms containing various powers of $u = E_e/E_{th}$ for $u \leq 10$. This fitting formula is given by,

$$\sigma_{nl}^{low} = \frac{1}{u(u+1)} \sum_{i=0}^{3} a_i u^i. \quad (u \leq 10) \quad [cm^2] \tag{24}$$

For higher energies we need different fitting formula as

$$\sigma_{nl}^{high} = \frac{1}{u(u+1)} \times 10^{\sum_{i=0}^{6} a_i u^i}. \quad (10 \leq u \leq 1000) \quad [cm^2] \tag{25}$$

Here a_i is a fitting parameter. The cross section fitting formula is used until $n \leq 10$ shell. Figures 24 and 25 show the photoionization cross sections and radiative recombination cross sections calculated for different l with fixed $n = 5$. The energy dependence of the PI cross section for $4d^8 5d^1$ near the threshold are flat and this feature produce the slow decay of the RR cross section at $E_e > 100$eV. The radiative recombination cross section for $n > 10$ shells is estimated using the semiclassical Kramers formula[7].

$$\sigma_n(x) = 2.1 \times 10^{-22} \frac{n}{x(x+1)}, \qquad (x = E_e/E_0) \quad [cm^2] \tag{26}$$

where n is the principle quantum number, $E_0 = z^2 Ry/n^2$, Ry is the Rydberg energy, and z is the residual charge of the ion. The Maxwellian averaged rate coefficients of the partial n shells are calculated numerically using the cross sections for the temperature range $10^{-3} - 10^{3}$eV.

$$K_{rr}^{nl}(T_e) = 6.6941 \times 10^{-14}\sqrt{E_{nl}}\beta^{3/2}\int_0^\infty u\sigma_{nl}(u)e^{-\beta u}du, \tag{27}$$

where $\beta = E_n/kT_e$ and $\sigma_{nl}(u) = \sigma_{nl}^{low}(u) + \sigma_{nl}^{high}(u)$. Figure 26 shows the temperature dependence of the radiative recombination rate coefficients calculated for different l with fixed $n = 5$. Figure 27 shows the radiative recombination rate coefficients summed over all l but each different n as a function of the electron temperature. The value of the radiative recombination rate coefficient decreases with increasing n. Also the difference of the values between n and $n+1$ of the radiative recombination rate coefficients decreases as n value increases. Thus, the total radiative recombination rate coefficient into all states of the Xe^{9+} ions can be written in the form

$$K_{rr}^{tot}(T_e) = \sum_{n=4}^{10} K_{rr}^{n}(T_e) + \sum_{n=11}^{1000} 5.18 \times 10^{-14} \times z\beta'^{3/2}e^{-\beta'}E_1(\beta'), \qquad [cm^3s^{-1}] \tag{28}$$

where $\beta' = \frac{z^2 Ry}{n^2 kT_e}$. Figure 28 shows the total radiative recombination rate coefficient represented by the solid line and the total dielectronic recombination rate coefficient represented by the dotted line. Through the figure, we know that the value of the radiative recombination rate coefficient is smaller than the value of the dielectronic recombination rate coefficient in our interest temperature region at Te = 1eV - 1000eV.

6. Summary

We calculated the energy levels, the radiative transition probabilities (Ar), autoionization rates (Aa), the intensity factors (Qd) of the dielectronic satellite spectra of Xe^{9+}, and the dielectric and radiative recombination rate coefficients of Xe^{10+} ion by the use of FAC code. We took into account the $4d^7 4f^1 nl$ states and the $4d^7 5p^1 nl$ states of Xe^{9+} ions. We investigated the l- and n-dependence for Ar and Aa. The values of Aa decrease as l increases for large l, but the values of Ar keep almost constant for large l. The Ar

values for the $4d^7 4f^1 nl \rightarrow 4d^8 nl$ and the $4d^7 5p^1 nl \rightarrow 4d^8 nl$ processes keep constant as n increases, respectively and the Aa values decrease as the n values increase. The values of Ar for the transitions of $4d^7 4f^1 nl \rightarrow 4d^8 nl$ are much larger than those for the transition $4d^7 5p^1 nl \rightarrow 4d^8 nl$ for the Xe^{9+}. We obtained the Aa values by the extrapolation according to scaled factor n^{-3} for $n > 15$. We obtained the dielectronic recombination, the direct excitation, the radiative recombination rate coefficients of Xe^{10+} using the FAC Code and compared these results. Also we obtained the satellite lines from Xe^{9+} ions. Through these results, we could know that the total dielectronic recombination rate coefficients have the maximum values at around 50eV. The temperatures at maximum values of dielectronic recombination rate coeficients move towards higher electron temperature with larger n and l. The dielectronic satellite lines of Xe^{9+} ions appear near the excitation lines of Xe^{10+} ions and the intensities of the dielectronic satellite lines can not be ignored at low temperate $Te < 10eV$. For identification of the spectrum from the highly charged ions, we need the information of the direct excitation of the parent ions. By our calculation, the radiative recombination rate coefficient is found smaller than the values of the dielectronic recombination processes in our interest temperature region at Te = 1eV - 1000eV.

Acknowledgment

One of the authors(M.-Y. Song) acknowledges Professor Y. -D. Jung and Professor R. M. More for useful discussions on atomic collisions and for M. F. Gu for guidance about the FAC code.

Reference

[1] A. Burgess, Astrophys. J. **139** (1964) 776

[2] J. N. Gau, Y. Hahn, and J. A Retter, J. Quant. Spectrosc. Radiat. Transfer **23** (1980) 131

[3] U. Fano and J. W. Copper, Rev. Mod. Phys. **40** (1968) 441

[4] K. Moribayashi and T. Kato, NIFS-DATA-36 (1964)

[5] R. K. Janev, L. P. Presnyakov, and V. P.Shevelko, "Physics of Highly Charged Ions", Springer-Verlag,Berlin Heideberg (1985)

[6] M. F. Gu, Astrophys. J. **590** (2003) 1131

[7] M. F. Gu, Astrophys. J. **589** (2003) 1085

[8] M. F. Gu, Astrophys. J. **582** (2003) 1241

[9] J. Oreg, W. H. Goldstein, M. Klapisch, and A. Bar-Shalom, Phys. Rev. A **44** (1991) 1750

[10] A. Sasaki, "HULLAC Code result" (2004)

[11] R. D. Cowan, "The Theory of Atomic Structure and Spectra", (University of California Press, Berkeley 1981)

[12] H. R. Griem, "Principles of Plasma Spectroscopy" (Cambridge University Press, New York, 1997)

[13] S. S. Churilov and Y. N. Yoshi, Phys. Scr. **65** (2002) 40

[14] D. A. Verner, D. G. Yakovlev, I. M. Band, and M. B. Trzhaskovskaya, At. Data Nucl. Data Table, **55** (1993) 233

Table 1: Energy levels of $4p^6 4d^8 (Xe^{10+})$ ions. The energy of these levels is measured from the ground level $(4p^6 4d^9)$ of the Xe^{9+} ion

No	conf	2J	energy (eV)	No	conf	2J	energy (eV)
0	$4d^8\ ^3F$	8	200.9630	5	$4d^8\ ^3P$	2	205.6899
1	$4d^8\ ^3F$	4	202.7772	6	$4d^8\ ^1G$	8	206.3526
2	$4d^8\ ^3F$	6	202.8800	7	$4d^8\ ^1D$	4	206.5961
3	$4d^8\ ^3P$	4	204.5248	8	$4d^8\ ^1S$	0	212.6528
4	$4d^8\ ^3P$	0	205.3987				

Table 2: Comparison of the averaged radiative transition $(4d^8nd - 4d^74f^1nd)$ rate $(\bar{A}r)$ and autoioization rate $(\bar{A}a)$ calculated with different theoretical models. [a : FAC, b : HULLAC]

conf	g_i^a	$\bar{A}r^a$	$\bar{A}a^a$	g_i^b	$\bar{A}r^b$	$\bar{A}a^b$
5d	16800	1.4141E+11	6.7229E+13	16800	1.3787E+11	5.8371E+13
6d	16782	1.4287E+11	2.5382E+13	16800	1.3824E+11	2.5419E+13
7d	16800	1.4315E+11	1.2001E+13	16800	1.3800E+11	1.2817E+13
8d	16800	1.4334E+11	6.8535E+12	16800	1.3817E+11	7.5536E+12

Table 3: Comparison of the averaged radiative transition $(4d^8nd - 4d^75p^1nd)$ rate $(\bar{A}r)$ and autoioization rate $(\bar{A}a)$ calculated with different theoretical models. [a : FAC, b : HULLAC]

conf	g_i^a	$\bar{A}r^a$	$\bar{A}a^a$	g_i^b	$\bar{A}r^b$	$\bar{A}a^b$
5d	7200	6.0882E+9	1.2834E+13	7200	2.1917E+10	1.7377E+13
6d	7200	2.6770E+10	5.6162E+12	7200	2.2010E+10	5.7613E+12
7d	7200	2.7252E+10	2.4710E+12	7200	2.3079E+10	2.5375E+12
8d	7200	2.7447E+10	1.3579E+12	7200	2.3058E+10	1.3906E+12

Table 4: Atomic data of λ, Ar, Aa, δE_{if},and Qd for the transition from the states of $4d^7 4f^2$ to $4d^8 4f$ with the initial states $4d^8 (i_0 = 0)$ of the Xe^{10+} ions

λ	g_i - g_f	Ar	Aa	δE_{if}	Qd
112.3256	16 - 14	1.1880E+12	1.8411E+13	2.4565	1.3937E+13
108.6254	16 - 16	9.7740E+11	1.8411E+13	2.4565	1.1466E+13
110.7701	12 - 12	9.0647E+11	7.1698E+13	0.2142	1.0563E+13
109.7990	14 - 14	1.0667E+12	2.9410E+13	4.9939	7.5012E+12
111.1275	14 - 12	9.9632E+11	2.9410E+13	4.9939	7.0062E+12
111.1176	10 - 10	7.6046E+11	8.8565E+12	0.1612	6.2052E+12
116.1126	10 - 08	3.2075E+12	1.1358E+15	18.3110	5.9133E+12
112.3154	08 - 08	7.2751E+11	3.6753E+13	1.1771	5.5277E+12
116.7137	08 - 06	1.9127E+12	1.9989E+15	16.4150	5.4110E+12
109.4017	12 - 10	4.3356E+11	7.1698E+13	0.2142	5.0525E+12
112.1833	10 - 10	7.2030E+11	2.8429E+12	1.3699	4.3169E+12
112.4071	08 - 08	6.2429E+11	9.6126E+12	0.9443	4.2096E+12
110.6317	12 - 10	4.2306E+11	6.3152E+12	0.6500	3.8684E+12
111.9503	06 - 08	7.1822E+11	1.4618E+13	1.3917	3.7849E+12
111.2572	12 - 12	3.9660E+11	6.3152E+12	0.6500	3.6264E+12
112.0110	06 - 06	6.5035E+11	1.4618E+13	1.3917	3.4273E+12
111.5374	10 - 10	3.3689E+11	2.2566E+13	1.8166	3.1188E+12
110.7998	06 - 06	5.4043E+11	3.0585E+13	0.1171	3.0501E+12
111.3671	02 - 04	1.5798E+12	2.1603E+13	0.8514	2.8919E+12
112.1630	06 - 06	5.1542E+11	1.5692E+13	0.8657	2.7475E+12
111.6379	04 - 04	8.1421E+11	9.4219E+12	0.5800	2.6955E+12
116.1234	06 - 04	1.3133E+12	1.3578E+15	11.1960	2.6569E+12
111.6982	08 - 08	4.1758E+11	7.2696E+12	1.6386	2.6413E+12
111.5876	02 - 02	1.3948E+12	3.3685E+13	0.1267	2.6362E+12
113.2904	08 - 06	3.6708E+11	1.6044E+13	0.7697	2.6185E+12
111.7284	06 - 06	2.1783E+12	1.1435E+14	21.1590	2.6153E+12
111.8796	02 - 04	1.8651E+12	5.8164E+13	4.4784	2.5964E+12
118.2161	08 - 08	9.1097E+11	1.9989E+15	16.4150	2.5771E+12
108.9116	12 - 10	2.0626E+11	7.1698E+13	0.2142	2.4036E+12
110.7800	04 - 04	6.2820E+11	3.3285E+13	0.1566	2.3720E+12
112.4683	06 - 06	8.1970E+11	3.3557E+13	3.5497	2.3566E+12
111.1774	06 - 06	4.4136E+11	1.5692E+13	0.8657	2.3527E+12
109.5467	08 - 06	3.1040E+11	2.5545E+13	0.1789	2.3058E+12
113.8313	12 - 10	1.9540E+11	7.1698E+13	0.2142	2.2771E+12
111.3971	08 - 08	8.3674E+11	2.9339E+12	3.3629	2.2708E+12
111.2871	10 - 10	6.9726E+11	2.5591E+13	4.3542	2.2608E+12
119.0789	10 - 08	2.3737E+11	2.2566E+13	1.8166	2.1975E+12
114.0721	08 - 10	3.4700E+11	7.2696E+12	1.6386	2.1948E+12
113.2387	12 - 12	1.8800E+11	7.1698E+13	0.2142	2.1908E+12
109.3921	12 - 12	2.3942E+11	6.3152E+12	0.6500	2.1892E+12
111.6178	08 - 08	3.0641E+11	1.6044E+13	0.7697	2.1858E+12

Table 4: Continued

λ	g_i - g_f	Ar	Aa	δE_{if}	Qd
109.9353	08 - 08	3.0396E+11	1.6044E+13	0.7697	2.1683E+12
113.7164	08 - 08	1.5598E+12	3.2555E+13	6.7253	2.1605E+12
111.1674	06 - 06	1.0346E+12	5.9438E+12	3.4634	1.9410E+12
111.7284	10 - 10	2.0789E+11	2.2566E+13	1.8166	1.9246E+12
109.1994	10 - 08	2.3068E+11	8.8565E+12	0.1612	1.8823E+12
110.2481	10 - 08	2.5353E+11	5.2883E+12	0.4503	1.8786E+12
114.3879	10 - 12	2.0106E+11	2.2566E+13	1.8166	1.8613E+12
113.5914	10 - 10	2.5113E+11	5.2883E+12	0.4503	1.8608E+12
111.0181	08 - 08	2.4996E+11	2.5545E+13	0.1789	1.8568E+12
111.4572	02 - 02	1.5896E+12	3.0709E+13	2.7983	1.8226E+12
113.4874	06 - 08	4.6710E+11	5.5642E+13	2.4600	1.8053E+12
112.0718	04 - 04	4.7244E+11	3.3285E+13	0.1566	1.7839E+12
112.8675	08 - 08	2.3034E+11	3.6753E+13	1.1771	1.7501E+12
112.7854	12 - 12	1.8511E+11	6.3152E+12	0.6500	1.6926E+12
111.8191	04 - 04	7.5521E+11	3.9501E+13	2.3510	1.6690E+12
111.3071	10 - 10	2.1945E+11	5.2883E+12	0.4503	1.6261E+12
112.2138	10 - 08	1.7520E+11	2.2566E+13	1.8166	1.6219E+12
110.5134	08 - 08	2.1257E+11	2.5545E+13	0.1789	1.5790E+12
112.2951	04 - 06	5.9883E+11	6.9492E+13	3.7124	1.5732E+12
109.4211	10 - 08	1.6892E+11	2.2566E+13	1.8166	1.5638E+12
113.2180	10 - 10	1.9108E+11	8.8565E+12	0.1612	1.5592E+12
112.7957	08 - 08	4.2369E+11	4.4860E+13	3.1321	1.4911E+12
117.1106	06 - 04	1.7915E+12	7.6792E+14	17.7530	1.4688E+12
110.8989	04 - 04	8.2300E+11	1.9508E+13	2.5651	1.4578E+12
110.8196	06 - 04	2.5254E+11	3.0585E+13	0.1171	1.4253E+12
112.6624	04 - 04	5.4123E+11	6.9492E+13	3.7124	1.4218E+12
115.8414	10 - 12	1.9162E+11	5.2883E+12	0.4503	1.4198E+12
118.4306	04 - 04	1.4973E+12	6.7547E+14	9.1143	1.4067E+12
111.5575	04 - 02	3.6904E+11	3.3285E+13	0.1566	1.3935E+12
113.0940	06 - 08	1.1575E+12	1.1435E+14	21.1590	1.3897E+12
111.7586	04 - 04	2.1675E+12	8.2708E+13	22.8290	1.3864E+12
115.5499	08 - 10	1.8775E+11	1.6044E+13	0.7697	1.3393E+12
113.1250	10 - 10	1.7894E+11	5.2883E+12	0.4503	1.3259E+12
109.1802	08 - 08	1.7741E+11	2.5545E+13	0.1789	1.3179E+12
114.4512	08 - 06	2.0663E+11	7.2696E+12	1.6386	1.3070E+12
111.5675	06 - 06	3.3692E+11	5.5642E+13	2.4600	1.3022E+12
110.6811	10 - 10	4.2966E+11	3.5114E+13	2.6766	1.2952E+12
110.4150	10 - 08	3.9655E+11	2.5591E+13	4.3542	1.2858E+12
111.3971	08 - 08	7.7605E+11	9.1437E+12	4.5081	1.2775E+12
110.0231	08 - 08	2.0161E+11	7.2696E+12	1.6386	1.2752E+12
111.1076	12 - 10	1.3517E+11	6.3152E+12	0.6500	1.2360E+12
115.1207	12 - 10	1.3240E+11	6.3152E+12	0.6500	1.2106E+12

Table 4: Continued

λ	g_i - g_f	Ar	Aa	δE_{if}	Qd
113.4044	08 - 10	1.6250E+11	2.5545E+13	0.1789	1.2071E+12
111.1574	10 - 10	5.1702E+11	2.0550E+13	2.8358	1.1847E+12
110.2873	10 - 08	1.9708E+11	2.8429E+12	1.3699	1.1812E+12
113.5914	06 - 06	3.0013E+11	5.5642E+13	2.4600	1.1600E+12
111.2672	08 - 06	4.2652E+11	2.9339E+12	3.3629	1.1575E+12
111.0181	10 - 08	1.9062E+11	2.8429E+12	1.3699	1.1424E+12
112.1123	06 - 04	2.0182E+11	3.0585E+13	0.1171	1.1390E+12
122.7453	06 - 06	5.5698E+11	1.3578E+15	11.1960	1.1268E+12
118.1034	10 - 08	3.7217E+11	3.5114E+13	2.6766	1.1219E+12
111.2173	06 - 08	3.7253E+11	3.3557E+13	3.5497	1.0710E+12
114.1877	12 - 14	1.1485E+11	6.3152E+12	0.6500	1.0502E+12
113.9254	10 - 08	1.2763E+11	8.8565E+12	0.1612	1.0414E+12
110.8890	08 - 08	2.9489E+11	4.4860E+13	3.1321	1.0378E+12
111.7485	10 - 12	1.2463E+11	8.8565E+12	0.1612	1.0170E+12

Table 5: Atomic data of λ, Ar, Aa, δE_{if},and Qd for the transition from the states of $4d^7 4f^2$ to $4d^8 4f$ with the initial states $4d^8 (i_0 = 4)$ of the Xe^{10+} ions

λ	g_f - g_i	Ar	Aa	δE_{if}	Qd
116.1126	10 - 08	3.2075E+12	3.8426E+14	13.8500	2.0006E+12
111.3971	08 - 08	7.7605E+11	1.1650E+13	0.0471	1.6276E+12
116.2541	08 - 06	3.1539E+12	1.8610E+14	15.7950	7.5665E+11
108.5873	08 - 06	3.1571E+11	1.1650E+13	0.0471	6.6215E+11
109.5467	08 - 06	1.8977E+11	1.1650E+13	0.0471	3.9801E+11
110.6910	10 - 10	9.0151E+11	7.2473E+12	1.0212	3.6172E+11
110.2677	08 - 08	1.7173E+11	1.1650E+13	0.0471	3.6018E+11
110.4347	10 - 08	7.0019E+11	7.2473E+12	1.0212	2.8094E+11
111.6580	08 - 10	1.2984E+11	1.1650E+13	0.0471	2.7232E+11
110.1306	08 - 06	1.2105E+11	1.1650E+13	0.0471	2.5388E+11
109.5467	08 - 08	1.0349E+11	1.1650E+13	0.0471	2.1705E+11
116.7137	08 - 06	1.9127E+12	5.9887E+13	11.9540	1.6211E+11
111.4973	08 - 06	7.2234E+10	1.1650E+13	0.0471	1.5150E+11
107.6539	08 - 06	6.1787E+10	1.1650E+13	0.0471	1.2959E+11
111.1375	08 - 10	5.1793E+10	1.1650E+13	0.0471	1.0863E+11
118.2161	08 - 08	9.1097E+11	5.9887E+13	11.9540	7.7211E+10
116.1126	08 - 06	3.4844E+10	1.1650E+13	0.0471	7.3080E+10
108.9403	08 - 06	3.3348E+10	1.1650E+13	0.0471	6.9942E+10
108.6063	10 - 08	1.5680E+11	7.2473E+12	1.0212	6.2913E+10
110.1697	10 - 10	1.5464E+11	7.2473E+12	1.0212	6.2047E+10
94.3354	10 - 10	9.6379E+10	3.8426E+14	13.8500	6.0114E+10
93.9707	10 - 10	7.9684E+10	3.8426E+14	13.8500	4.9701E+10
106.8744	08 - 08	2.1064E+10	1.1650E+13	0.0471	4.4178E+10
105.7081	08 - 06	2.0097E+10	1.1650E+13	0.0471	4.2150E+10
109.0266	08 - 08	1.8953E+10	1.1650E+13	0.0471	3.9751E+10
107.0775	10 - 08	8.5347E+10	7.2473E+12	1.0212	3.4244E+10
108.8829	08 - 08	1.4688E+10	1.1650E+13	0.0471	3.0806E+10
94.9567	08 - 08	1.2152E+11	1.8610E+14	15.7950	2.9154E+10
93.1378	10 - 10	4.1440E+10	3.8426E+14	13.8500	2.5847E+10
111.7284	06 - 06	2.1783E+12	1.0875E+12	16.6980	2.4872E+10
107.2906	08 - 08	1.1051E+10	1.1650E+13	0.0471	2.3178E+10
109.5177	08 - 10	1.0096E+10	1.1650E+13	0.0471	2.1175E+10

Table 5: Continued

λ	g_i - g_f	Ar	Aa	δE_{if}	Qd
111.7586	04 - 04	2.1675E+12	1.1720E+12	18.3680	1.9646E+10
95.5127	10 - 08	3.1476E+10	3.8426E+14	13.8500	1.9632E+10
94.1063	08 - 08	7.6361E+10	1.8610E+14	15.7950	1.8320E+10
109.2283	10 - 12	4.3210E+10	7.2473E+12	1.0212	1.7337E+10
105.5102	08 - 06	8.2080E+09	1.1650E+13	0.0471	1.7215E+10
109.3246	10 - 08	4.2626E+10	7.2473E+12	1.0212	1.7103E+10
108.0950	10 - 08	4.0887E+10	7.2473E+12	1.0212	1.6405E+10
113.7164	08 - 08	1.5598E+12	2.1350E+11	2.2642	1.4169E+10
111.8796	02 - 04	1.8651E+12	3.1436E+11	0.0173	1.4033E+10
107.9633	10 - 08	3.4105E+10	7.2473E+12	1.0212	1.3684E+10
113.0940	06 - 08	1.1575E+12	1.0875E+12	16.6980	1.3216E+10
113.5082	04 - 06	1.3265E+12	1.1720E+12	18.3680	1.2023E+10

Table 6: Atomic data of λ, Ar, Aa, δE_{if},and Qd for the transition from the states of $4d^7 4f^2$ to $4d^8 4f$ with the initial states $4d^8(i_0 = 6)$ of the Xe^{10+} ions

λ	g_i - g_f	Ar	Aa	δE_{if}	Qd
110.6910	10 - 10	9.0151E+11	1.3053E+14	0.0662	6.5148E+12
110.4347	10 - 08	7.0019E+11	1.3053E+14	0.0662	5.0600E+12
111.7284	06 - 06	2.1783E+12	1.4127E+14	15.7430	3.2310E+12
118.2837	02 - 02	1.8143E+12	1.7225E+15	4.9248	3.1423E+12
113.7164	08 - 08	1.5598E+12	4.7197E+13	1.3092	3.1321E+12
118.4306	04 - 04	1.4973E+12	1.4652E+15	3.6982	3.0513E+12
111.7586	04 - 04	2.1675E+12	1.8135E+14	17.4130	3.0399E+12
118.6573	02 - 04	1.9081E+12	1.7386E+15	3.4988	2.8112E+12
114.0407	06 - 06	1.4901E+12	1.1313E+14	1.0278	2.3968E+12
116.1234	06 - 04	1.3133E+12	1.1703E+15	5.7803	2.2900E+12
117.1106	06 - 04	1.7915E+12	1.1818E+15	12.3370	2.2604E+12
116.7137	08 - 06	1.9127E+12	7.8725E+14	10.9990	2.1311E+12
116.7797	04 - 02	1.2355E+12	1.7065E+15	6.2749	2.0641E+12
113.5082	04 - 06	1.3265E+12	1.8135E+14	17.4130	1.8604E+12
113.0940	06 - 08	1.1575E+12	1.4127E+14	15.7430	1.7169E+12
116.2541	08 - 06	3.1539E+12	4.0010E+14	14.8400	1.6267E+12
116.1126	10 - 08	3.2075E+12	2.6120E+14	12.8950	1.3599E+12
108.6063	10 - 08	1.5680E+11	1.3053E+14	0.0662	1.1331E+12
110.1697	10 - 10	1.5464E+11	1.3053E+14	0.0662	1.1175E+12
118.2161	08 - 08	9.1097E+11	7.8725E+14	10.9990	1.0150E+12
122.7453	06 - 06	5.5698E+11	1.1703E+15	5.7803	9.7120E+11
119.0446	06 - 06	7.4322E+11	1.1818E+15	12.3370	9.3773E+11
124.2260	04 - 04	5.2366E+11	1.7065E+15	6.2749	8.7484E+11
125.3323	04 - 06	3.6552E+11	1.4652E+15	3.6982	7.4489E+11
106.2061	06 - 04	4.5251E+11	1.4127E+14	15.7430	6.7119E+11
107.0775	10 - 08	8.5347E+10	1.3053E+14	0.0662	6.1676E+11
124.4030	06 - 08	3.1487E+11	1.1703E+15	5.7803	5.4903E+11
101.6771	04 - 02	2.4941E+11	1.4652E+15	3.6982	5.0827E+11
105.6901	04 - 02	3.5109E+11	1.8135E+14	17.4130	4.9239E+11
113.6330	04 - 06	1.6682E+12	1.1310E+13	1.4200	4.5903E+11
126.4005	04 - 06	2.7010E+11	1.7065E+15	6.2749	4.5124E+11
100.6699	02 - 02	2.1633E+11	1.7225E+15	4.9248	3.7468E+11
113.7373	06 - 08	1.6568E+12	7.3624E+12	1.2904	3.5671E+11
115.2705	06 - 06	2.6290E+11	1.1818E+15	12.3370	3.3170E+11

Table 6: Continued

λ	g_i - g_f	Ar	Aa	δE_{if}	Qd
125.9293	02 - 04	1.8719E+11	1.7225E+15	4.9248	3.2421E+11
109.2283	10 - 12	4.3210E+10	1.3053E+14	0.0662	3.1226E+11
109.3246	10 - 08	4.2626E+10	1.3053E+14	0.0662	3.0804E+11
105.0453	04 - 04	1.7874E+11	1.7065E+15	6.2749	2.9861E+11
108.0950	10 - 08	4.0887E+10	1.3053E+14	0.0662	2.9547E+11
119.6882	04 - 02	1.3516E+11	1.4652E+15	3.6982	2.7544E+11
113.4666	06 - 04	1.8303E+11	1.4127E+14	15.7430	2.7148E+11
117.0553	02 - 04	1.5639E+11	1.7225E+15	4.9248	2.7086E+11
107.9633	10 - 08	3.4105E+10	1.3053E+14	0.0662	2.4646E+11
100.7680	02 - 04	1.6036E+11	1.7386E+15	3.4988	2.3626E+11
105.1701	06 - 06	1.3087E+11	1.1703E+15	5.7803	2.2820E+11
115.5822	04 - 04	1.1751E+11	1.7065E+15	6.2749	1.9632E+11
127.7801	02 - 04	1.2118E+11	1.7386E+15	3.4988	1.7854E+11
110.6416	10 - 12	2.1377E+10	1.3053E+14	0.0662	1.5448E+11
113.7477	08 - 06	7.4472E+10	4.7197E+13	1.3092	1.4954E+11
107.1793	06 - 04	8.9996E+10	1.1313E+14	1.0278	1.4476E+11
99.8912	02 - 04	7.8964E+10	1.7225E+15	4.9248	1.3676E+11
110.0719	04 - 06	9.2915E+10	1.8135E+14	17.4130	1.3031E+11
115.0353	10 - 08	1.7941E+10	1.3053E+14	0.0662	1.2965E+11
100.1333	04 - 02	6.1711E+10	1.4652E+15	3.6982	1.2576E+11
98.9268	06 - 04	7.1321E+10	1.1703E+15	5.7803	1.2436E+11
108.0103	08 - 06	6.0133E+10	4.7197E+13	1.3092	1.2075E+11
103.2950	06 - 06	9.2680E+10	1.1818E+15	12.3370	1.1694E+11
101.5355	04 - 06	5.2276E+10	1.4652E+15	3.6982	1.0653E+11
106.1879	06 - 08	6.4178E+10	1.1313E+14	1.0278	1.0323E+11
100.2953	02 - 02	7.0066E+10	1.7386E+15	3.4988	1.0323E+11
101.8441	02 - 02	6.9792E+10	1.7386E+15	3.4988	1.0283E+11
107.9727	10 - 10	1.3910E+10	1.3053E+14	0.0662	1.0052E+11

Table 7: Atomic data of λ, Ar, Aa, δE_{if},and Qd for the transition from the states of $4d^7 5p^1 5d$ to $4d^8 5d$ with the initial states $4d^8 (i_0 = 0)$ of the Xe^{10+} ions

λ	g_i - g_f	Ar	Aa	δE_{if}	Qd
136.0335	12 - 14	2.8240E+10	1.8705E+12	0.6925	3.3211E+11
137.8743	12 - 12	1.4691E+10	5.2908E+12	1.0691	1.7529E+11
136.1550	14 - 12	1.8071E+10	8.1933E+11	2.2047	1.6902E+11
135.1686	16 - 14	1.0363E+10	4.0768E+12	1.2757	1.6538E+11
135.9304	12 - 10	1.3595E+10	4.8785E+12	1.4661	1.6183E+11
137.6055	12 - 10	1.0834E+10	4.8785E+12	1.4661	1.2896E+11
139.5946	10 - 10	1.2273E+10	1.1367E+13	0.1823	1.2237E+11
134.9278	10 - 12	1.2122E+10	7.8055E+12	1.0038	1.2055E+11
138.3051	08 - 10	1.4574E+10	1.5396E+12	1.0103	1.1289E+11
136.6668	10 - 12	1.6306E+10	1.0032E+12	1.8637	1.1065E+11
136.8623	08 - 08	1.4442E+10	7.8948E+11	0.9897	1.0913E+11
136.7793	08 - 06	1.4031E+10	1.6962E+12	0.0138	1.0899E+11
134.8319	12 - 12	9.1012E+09	5.2908E+12	1.0691	1.0860E+11
137.3438	10 - 08	1.0417E+10	3.4116E+13	0.6721	1.0405E+11
133.3763	12 - 10	8.8221E+09	9.0028E+11	1.5005	1.0339E+11
136.4544	08 - 10	1.2718E+10	8.3050E+12	1.7172	1.0110E+11
134.4091	12 - 14	8.3287E+09	9.0648E+11	1.7940	9.6961E+10
139.0434	10 - 10	9.6936E+09	2.9013E+13	0.5343	9.6811E+10
136.1458	10 - 12	1.7211E+10	2.8667E+12	2.2108	9.6555E+10
133.7600	12 - 10	1.3076E+10	2.1154E+12	3.5474	9.5191E+10
136.7718	12 - 12	8.1313E+09	9.0648E+11	1.7940	9.4663E+10
137.1822	06 - 08	1.6492E+10	9.0421E+11	1.5801	9.3679E+10
136.1963	14 - 14	6.8670E+09	2.3417E+11	0.5835	9.2290E+10
137.1065	12 - 10	7.9125E+09	9.0648E+11	1.7940	9.2116E+10
139.0380	10 - 12	9.2244E+09	2.6397E+12	0.3165	9.1161E+10
136.8324	12 - 10	7.1616E+09	4.8785E+12	1.4661	8.5247E+10
135.6857	08 - 06	1.0368E+10	8.3050E+12	1.7172	8.2421E+10
134.1094	10 - 10	1.1135E+10	9.5350E+12	2.7046	8.2031E+10
137.9314	08 - 10	1.0397E+10	2.0829E+12	1.2532	8.1767E+10
133.6220	08 - 08	1.0470E+10	1.5396E+12	1.0103	8.1100E+10
135.2289	12 - 10	7.0135E+09	1.0479E+12	0.2270	8.0943E+10
133.7219	10 - 10	7.9616E+09	9.6906E+11	1.2602	7.7297E+10
136.2495	10 - 10	7.7472E+09	7.9710E+12	1.2525	7.7205E+10
134.0928	10 - 10	7.6842E+09	7.8055E+12	1.0038	7.6415E+10
137.5938	10 - 12	7.6000E+09	7.9710E+12	1.2525	7.5738E+10
136.0282	06 - 06	1.3199E+10	9.2648E+11	1.8325	7.4810E+10
136.6327	10 - 08	7.4305E+09	7.8055E+12	1.0038	7.3892E+10
136.9723	06 - 08	1.2305E+10	5.1125E+12	1.7185	7.3160E+10
138.2743	10 - 08	7.1308E+09	3.3983E+13	0.0646	7.1257E+10
131.5228	10 - 12	7.1566E+09	2.8079E+12	0.8234	7.0552E+10
136.0254	10 - 08	7.0797E+09	5.6663E+12	1.5471	7.0367E+10
134.2371	12 - 10	6.2641E+09	7.3999E+12	2.6167	7.0242E+10

Table 7: Continued

λ	g_i - g_f	Ar	Aa	δE_{if}	Qd
135.8550	08 - 08	9.0270E+09	1.5884E+12	1.0736	7.0241E+10
136.4337	10 - 08	7.3223E+09	8.9232E+11	0.7396	6.9816E+10
135.1088	08 - 08	8.8803E+09	2.7467E+12	1.6308	6.9537E+10
135.3864	12 - 12	5.8891E+09	1.8705E+12	0.6925	6.9258E+10
134.7271	08 - 10	1.0629E+10	2.3601E+13	2.8820	6.6851E+10
133.0204	12 - 10	5.7686E+09	1.0479E+12	0.2270	6.6576E+10
135.6951	08 - 08	8.4810E+09	2.7467E+12	1.6308	6.6410E+10
135.9446	10 - 12	6.4628E+09	2.6397E+12	0.3165	6.3869E+10
133.2984	12 - 14	5.2588E+09	2.1263E+14	2.5626	6.2772E+10
135.5573	08 - 10	7.8220E+09	8.3050E+12	1.7172	6.2181E+10
138.8044	08 - 10	8.1714E+09	5.8934E+11	0.1789	6.1916E+10
136.4282	06 - 08	1.0355E+10	1.5408E+12	1.2780	6.0907E+10
136.3080	10 - 08	6.1446E+09	2.8079E+12	0.8234	6.0576E+10
136.0782	12 - 12	5.2008E+09	1.0479E+12	0.2270	6.0023E+10
133.8844	10 - 12	9.1854E+09	1.9286E+13	3.7491	6.0010E+10
137.4032	08 - 08	7.5003E+09	3.3378E+12	0.0984	5.9422E+10
135.8098	10 - 10	5.9215E+09	5.6663E+12	1.5471	5.8856E+10
135.9591	10 - 08	5.7509E+09	7.8055E+12	1.0038	5.7189E+10
132.8572	10 - 10	8.3846E+09	1.0032E+12	1.8637	5.6897E+10
138.0421	10 - 10	5.6911E+09	3.4116E+13	0.6721	5.6844E+10
135.7396	10 - 10	7.7131E+09	9.5350E+12	2.7046	5.6822E+10
134.0287	08 - 10	8.1505E+09	8.3552E+12	2.7603	5.6718E+10
131.5929	08 - 10	8.1019E+09	8.3552E+12	2.7603	5.6380E+10
133.2210	12 - 14	5.0250E+09	7.3999E+12	2.6167	5.6347E+10
137.9207	10 - 10	5.6497E+09	9.6906E+11	1.2602	5.4851E+10
137.8025	12 - 10	4.7484E+09	1.0479E+12	0.2270	5.4802E+10
138.0814	04 - 02	1.6431E+10	2.5838E+11	0.2348	5.4613E+10
135.3501	10 - 08	7.9420E+09	1.0032E+12	1.8637	5.3893E+10
134.8295	10 - 10	5.3410E+09	6.3533E+13	0.4986	5.3384E+10
137.0784	06 - 06	9.2475E+09	8.6631E+11	1.1342	5.3030E+10
134.2054	10 - 12	5.6674E+09	9.2625E+13	3.5276	5.2876E+10
136.5843	08 - 10	6.6408E+09	2.7467E+12	1.6308	5.2000E+10
135.5633	08 - 06	6.5174E+09	2.7467E+12	1.6308	5.1034E+10
136.6626	10 - 08	5.1068E+09	2.9013E+13	0.5343	5.1002E+10
138.3094	10 - 10	5.1022E+09	6.3533E+13	0.4986	5.0997E+10
138.3710	06 - 06	2.4183E+10	6.8425E+13	5.9456	5.0961E+10
137.0628	12 - 14	4.2724E+09	1.1557E+12	0.0081	5.0684E+10
136.0042	06 - 08	8.5666E+09	2.3356E+12	1.4231	5.0273E+10
135.2321	10 - 08	4.9944E+09	5.6663E+12	1.5471	4.9641E+10
138.3834	08 - 10	6.2278E+09	1.0518E+13	0.4506	4.9544E+10
134.6779	08 - 10	8.1481E+09	3.9568E+12	2.3144	4.9197E+10
138.2212	04 - 02	1.4990E+10	2.4617E+11	1.0386	4.8846E+10

Table 7: Continued

λ	g_i - g_f	Ar	Aa	δE_{if}	Qd
138.4995	12 - 10	4.0299E+09	1.0088E+13	0.8845	4.8310E+10
135.7956	14 - 14	3.4848E+09	2.8853E+11	0.8522	4.8102E+10
137.7501	08 - 06	6.2282E+09	5.8934E+11	0.1789	4.7192E+10
137.0316	10 - 08	4.8964E+09	8.9232E+11	0.7396	4.6686E+10
137.5929	08 - 06	5.8502E+09	1.0518E+13	0.4506	4.6540E+10
137.1703	08 - 06	5.9747E+09	1.5884E+12	1.0736	4.6491E+10
138.3404	10 - 08	4.6983E+09	2.8079E+12	0.8234	4.6317E+10
131.8338	10 - 12	4.7947E+09	2.3902E+14	3.1604	4.6315E+10
137.9385	10 - 10	4.8499E+09	8.9232E+11	0.7396	4.6242E+10
137.0931	08 - 06	6.0766E+09	6.6924E+11	0.0543	4.5940E+10
138.2542	10 - 10	4.5912E+09	2.9013E+13	0.5343	4.5853E+10
137.2525	08 - 10	5.7919E+09	3.0145E+12	1.1888	4.5839E+10
136.1239	06 - 06	7.6466E+09	2.3356E+12	1.4231	4.4874E+10
133.7887	10 - 10	4.7728E+09	9.2625E+13	3.5276	4.4530E+10
138.3815	10 - 12	4.6516E+09	8.9232E+11	0.7396	4.4352E+10
136.8176	08 - 10	5.5381E+09	1.9947E+13	1.4760	4.4268E+10
136.1985	06 - 06	7.4061E+09	5.1125E+12	1.7185	4.4033E+10
135.4165	10 - 12	4.4017E+09	3.4116E+13	0.6721	4.3965E+10
137.3545	08 - 10	5.5908E+09	2.7467E+12	1.6308	4.3778E+10
135.6207	10 - 12	4.3715E+09	2.9013E+13	0.5343	4.3659E+10
131.3210	10 - 12	4.6551E+09	9.2625E+13	3.5276	4.3432E+10
136.3221	08 - 10	7.1493E+09	3.9568E+12	2.3144	4.3166E+10
136.1572	06 - 08	7.1891E+09	2.3797E+13	0.8711	4.3090E+10
137.0996	08 - 10	5.4597E+09	1.1547E+12	0.6882	4.2616E+10
131.9019	12 - 14	5.8435E+09	2.1154E+12	3.5474	4.2540E+10
134.1003	06 - 08	7.8287E+09	5.6216E+11	0.6793	4.2430E+10
136.8690	08 - 08	5.3083E+09	1.0518E+13	0.4506	4.2229E+10
142.9119	08 - 06	7.4191E+09	5.7159E+12	3.0986	4.2215E+10
137.2916	06 - 04	7.3455E+09	8.4170E+11	0.2466	4.2028E+10
138.2902	08 - 08	5.5417E+09	6.6924E+11	0.0543	4.1896E+10
135.4851	04 - 06	1.1017E+10	9.1215E+11	1.1277	4.1770E+10
130.0134	12 - 12	3.6141E+09	1.0479E+12	0.2270	4.1711E+10
134.1347	10 - 12	4.1962E+09	5.6663E+12	1.5471	4.1707E+10
132.0660	08 - 06	5.2420E+09	1.0518E+13	0.4506	4.1701E+10
137.1240	10 - 10	4.1734E+09	3.4116E+13	0.6721	4.1685E+10
138.0674	08 - 10	5.4942E+09	6.6924E+11	0.0543	4.1537E+10
136.4950	08 - 06	5.1797E+09	1.0518E+13	0.4506	4.1206E+10
136.5175	06 - 08	7.0381E+09	1.1756E+12	0.6308	4.1001E+10
132.3603	12 - 12	3.4960E+09	1.0479E+12	0.2270	4.0348E+10
137.4477	06 - 08	7.9623E+09	2.5658E+11	0.0161	4.0257E+10
135.4765	08 - 10	6.3910E+09	2.3601E+13	2.8820	4.0196E+10
134.7243	12 - 10	3.3472E+09	1.4780E+14	2.2827	4.0022E+10

Table 7: Continued

λ	g_i - g_f	Ar	Aa	δE_{if}	Qd
137.4209	06 - 08	6.7014E+09	2.3356E+12	1.4231	3.9327E+10
135.5441	08 - 10	5.0561E+09	1.6962E+12	0.0138	3.9277E+10
137.3878	10 - 10	3.9128E+09	6.3533E+13	0.4986	3.9109E+10
137.4608	08 - 10	4.8894E+09	1.0518E+13	0.4506	3.8896E+10
142.1746	08 - 06	1.3904E+10	1.9338E+13	3.5485	3.8867E+10
136.7815	08 - 06	5.0086E+09	6.1525E+11	0.3150	3.8175E+10
137.5619	06 - 04	6.6987E+09	4.3343E+11	0.0691	3.7658E+10
132.6799	10 - 10	3.7661E+09	1.1367E+13	0.1823	3.7550E+10
138.7241	10 - 10	3.9148E+09	8.9232E+11	0.7396	3.7326E+10
137.1053	08 - 08	4.7294E+09	2.7467E+12	1.6308	3.7033E+10
138.3152	10 - 10	3.7167E+09	7.8055E+12	1.0038	3.6960E+10
138.8038	08 - 10	4.7255E+09	1.1547E+12	0.6882	3.6885E+10
137.4567	10 - 10	3.6894E+09	7.1875E+12	1.0546	3.6781E+10
137.1230	06 - 08	6.7851E+09	5.6216E+11	0.6793	3.6774E+10
133.3253	08 - 10	4.7218E+09	1.6962E+12	0.0138	3.6680E+10
136.6878	06 - 08	6.1409E+09	5.5284E+12	0.5176	3.6586E+10
132.1403	10 - 08	3.7004E+09	2.8079E+12	0.8234	3.6480E+10
139.7797	10 - 10	3.6383E+09	3.3983E+13	0.0646	3.6357E+10
137.8916	08 - 06	2.0303E+10	5.5407E+13	6.2572	3.6044E+10
132.9893	08 - 06	4.5703E+09	2.7467E+12	1.6308	3.5787E+10
137.1454	10 - 12	3.5772E+09	5.6663E+12	1.5471	3.5555E+10
136.5351	10 - 08	3.5467E+09	3.4116E+13	0.6721	3.5425E+10
139.6622	08 - 06	2.6594E+10	2.7630E+13	6.1448	3.5347E+10
133.4697	10 - 08	4.7828E+09	9.5350E+12	2.7046	3.5235E+10
135.7475	12 - 14	2.9203E+09	1.0088E+13	0.8845	3.5008E+10
133.3193	10 - 08	3.5034E+09	7.1875E+12	1.0546	3.4927E+10
138.0413	06 - 04	6.4370E+09	5.6216E+11	0.6793	3.4887E+10
131.6399	10 - 12	3.6589E+09	8.9232E+11	0.7396	3.4886E+10
138.3313	08 - 06	4.5217E+09	6.1525E+11	0.3150	3.4464E+10
139.0614	08 - 10	4.4311E+09	1.6962E+12	0.0138	3.4421E+10
133.7832	06 - 04	5.6974E+09	1.0004E+13	0.4562	3.4028E+10
135.6570	08 - 10	4.8856E+09	8.3552E+12	2.7603	3.3998E+10
135.0492	06 - 06	5.7710E+09	2.3356E+12	1.4231	3.3867E+10
136.3101	04 - 06	1.0088E+10	2.7624E+11	0.3258	3.3731E+10
135.1053	06 - 08	5.9383E+09	9.0421E+11	1.5801	3.3731E+10
136.3696	12 - 10	2.8099E+09	1.4780E+14	2.2827	3.3598E+10
136.1522	06 - 06	6.1725E+09	5.6216E+11	0.6793	3.3453E+10
134.5755	10 - 10	3.3485E+09	3.4116E+13	0.6721	3.3446E+10
135.5775	06 - 06	5.5819E+09	1.6599E+13	1.0653	3.3438E+10
136.6368	06 - 04	6.1313E+09	5.6216E+11	0.6793	3.3230E+10
135.7700	06 - 08	5.5846E+09	5.1125E+12	1.7185	3.3204E+10
135.2108	06 - 06	5.5375E+09	1.6599E+13	1.0653	3.3172E+10

Table 7: Continued

λ	g_i - g_f	Ar	Aa	δE_{if}	Qd
136.5203	08 - 06	4.3259E+09	7.8948E+11	0.9897	3.2688E+10
135.6837	08 - 08	4.0990E+09	3.0145E+12	1.1888	3.2441E+10
135.4139	08 - 08	4.5902E+09	8.3552E+12	2.7603	3.1942E+10
132.1678	08 - 10	5.2427E+09	2.0967E+13	4.6641	3.1612E+10
139.4101	06 - 08	5.3392E+09	2.2203E+12	0.1358	3.1511E+10
136.0385	12 - 12	2.6133E+09	1.4780E+14	2.2827	3.1247E+10
139.9762	06 - 06	1.4824E+10	6.8425E+13	5.9456	3.1239E+10
136.7888	08 - 08	3.9145E+09	1.0518E+13	0.4506	3.1141E+10
134.2523	12 - 12	2.6086E+09	4.8785E+12	1.4661	3.1051E+10
137.2977	08 - 06	4.0815E+09	7.8948E+11	0.9897	3.0841E+10
136.2107	06 - 08	5.2545E+09	2.3356E+12	1.4231	3.0836E+10
137.9232	04 - 06	9.2636E+09	2.5838E+11	0.2348	3.0790E+10
137.0218	10 - 10	3.2270E+09	8.9232E+11	0.7396	3.0768E+10
136.8023	06 - 06	5.3571E+09	8.4170E+11	0.2466	3.0651E+10
130.8343	12 - 10	2.6147E+09	9.0028E+11	1.5005	3.0644E+10
139.8689	12 - 10	2.5774E+09	1.1557E+12	0.0081	3.0576E+10
134.8124	06 - 08	5.3653E+09	9.2648E+11	1.8325	3.0410E+10
136.7436	08 - 06	3.9052E+09	1.5396E+12	1.0103	3.0249E+10
134.3853	04 - 04	7.9381E+09	9.0187E+11	1.8220	3.0217E+10
130.8817	12 - 10	2.5237E+09	4.8785E+12	1.4661	3.0041E+10
138.8436	10 - 08	2.9928E+09	6.3533E+13	0.4986	2.9914E+10
138.7039	08 - 08	3.7986E+09	1.4734E+12	0.5885	2.9847E+10
134.3549	10 - 10	3.0182E+09	2.8079E+12	0.8234	2.9754E+10
133.7008	12 - 14	2.4865E+09	1.4780E+14	2.2827	2.9731E+10
138.2075	08 - 10	3.8197E+09	1.5884E+12	1.0736	2.9722E+10
133.2667	04 - 06	7.8977E+09	6.2520E+11	0.9033	2.9677E+10
132.6165	12 - 10	2.5572E+09	1.0479E+12	0.2270	2.9513E+10
136.2913	06 - 04	5.1500E+09	9.2648E+11	1.8325	2.9189E+10
130.0651	12 - 10	2.4843E+09	9.0028E+11	1.5005	2.9116E+10
134.7362	08 - 08	6.4744E+09	9.5665E+11	1.8845	2.9063E+10
136.7319	12 - 14	2.5067E+09	1.0479E+12	0.2270	2.8930E+10
137.9105	08 - 06	3.6649E+09	1.4734E+12	0.5885	2.8796E+10
135.5882	08 - 08	3.6598E+09	2.0829E+12	1.2532	2.8782E+10
135.4377	08 - 06	6.4069E+09	9.5665E+11	1.8845	2.8760E+10
136.8849	06 - 06	5.0034E+09	8.4170E+11	0.2466	2.8627E+10
137.9997	06 - 06	5.6549E+09	2.5658E+11	0.0161	2.8591E+10
136.0439	04 - 06	7.5070E+09	9.0187E+11	1.8220	2.8576E+10
137.2001	08 - 08	3.7516E+09	5.8934E+11	0.1789	2.8426E+10
137.4602	06 - 04	4.8010E+09	2.2203E+12	0.1358	2.8334E+10
137.5286	06 - 08	5.5871E+09	2.5658E+11	0.0161	2.8248E+10
135.9510	12 - 10	2.3651E+09	2.1263E+14	2.5626	2.8231E+10
137.3224	08 - 08	3.5630E+09	3.3378E+12	0.0984	2.8228E+10

Table 7: Continued

λ	g_i - g_f	Ar	Aa	δE_{if}	Qd
134.8047	08 - 06	4.6720E+09	3.9568E+12	2.3144	2.8209E+10
136.3546	08 - 08	3.5586E+09	3.0145E+12	1.1888	2.8164E+10
131.5047	08 - 08	3.5603E+09	1.1547E+12	0.6882	2.7790E+10
139.7265	08 - 10	3.4995E+09	3.3378E+12	0.0984	2.7725E+10
133.3094	10 - 10	2.7765E+09	5.6663E+12	1.5471	2.7596E+10
136.3125	06 - 04	4.6236E+09	5.5284E+12	0.5176	2.7547E+10
136.7531	10 - 08	4.0388E+09	1.0032E+12	1.8637	2.7407E+10
137.4149	04 - 06	7.7101E+09	4.1005E+11	0.5673	2.7328E+10
132.1819	10 - 10	2.7109E+09	2.9013E+13	0.5343	2.7074E+10
138.1137	06 - 06	4.5037E+09	1.0004E+13	0.4562	2.6898E+10
139.6015	08 - 08	3.4567E+09	1.6962E+12	0.0138	2.6852E+10
137.8003	08 - 06	3.4508E+09	6.1525E+11	0.3150	2.6302E+10
137.2756	10 - 08	2.6372E+09	1.1367E+13	0.1823	2.6294E+10
136.3034	06 - 06	4.5575E+09	8.6631E+11	1.1342	2.6135E+10
134.6093	16 - 14	1.7405E+09	2.5573E+10	1.6568	2.6071E+10
135.9762	06 - 08	4.5837E+09	9.0421E+11	1.5801	2.6037E+10
135.2920	08 - 06	3.3473E+09	1.5396E+12	1.0103	2.5928E+10
135.7720	08 - 08	3.2440E+09	8.3050E+12	1.7172	2.5788E+10
131.5433	08 - 10	3.3963E+09	7.8948E+11	0.9897	2.5663E+10
130.7857	08 - 08	4.2458E+09	2.0967E+13	4.6641	2.5601E+10
137.8100	10 - 10	2.5821E+09	2.8079E+12	0.8234	2.5455E+10
135.9464	06 - 08	4.2471E+09	1.6599E+13	1.0653	2.5442E+10
136.5178	08 - 10	3.2679E+09	1.5884E+12	1.0736	2.5428E+10
135.6462	08 - 06	3.2625E+09	1.5884E+12	1.0736	2.5386E+10
137.0832	06 - 04	4.2773E+09	2.7915E+12	1.3070	2.5373E+10
135.6854	08 - 10	3.2366E+09	2.7467E+12	1.6308	2.5344E+10
136.1125	04 - 06	6.6596E+09	9.7498E+11	0.7059	2.5298E+10
132.1746	10 - 10	2.5587E+09	2.8079E+12	0.8234	2.5225E+10
137.0010	10 - 10	3.7057E+09	1.0032E+12	1.8637	2.5146E+10
139.3284	04 - 02	7.4866E+09	2.7624E+11	0.3258	2.5033E+10
132.3000	08 - 10	3.1425E+09	1.0518E+13	0.4506	2.4999E+10
137.5793	06 - 08	4.1613E+09	5.5284E+12	0.5176	2.4792E+10
136.6441	08 - 10	3.2636E+09	7.8948E+11	0.9897	2.4661E+10
137.3456	06 - 04	4.2727E+09	8.6631E+11	1.1342	2.4502E+10
135.7649	06 - 08	4.2726E+09	8.6631E+11	1.1342	2.4501E+10
135.6830	04 - 02	6.4213E+09	9.0187E+11	1.8220	2.4443E+10
138.2030	06 - 06	3.5553E+10	2.9651E+13	6.0546	2.4364E+10
137.4912	04 - 04	7.4475E+09	2.4617E+11	1.0386	2.4268E+10
136.7356	08 - 08	3.0942E+09	1.5884E+12	1.0736	2.4077E+10
135.6219	12 - 12	2.0143E+09	2.1263E+14	2.5626	2.4044E+10
135.2908	04 - 04	6.3130E+09	9.7498E+11	0.7059	2.3982E+10

Table 7: Continued

λ	g_i - g_f	Ar	Aa	δE_{if}	Qd
133.3938	08 - 06	3.9701E+09	3.9568E+12	2.3144	2.3971E+10
138.0932	10 - 08	2.3763E+09	1.1367E+13	0.1823	2.3693E+10
136.4549	10 - 08	2.4266E+09	9.6906E+11	1.2602	2.3559E+10
134.0210	08 - 06	3.0287E+09	1.6962E+12	0.0138	2.3527E+10
137.1760	08 - 06	3.1057E+09	6.6924E+11	0.0543	2.3480E+10
135.0247	10 - 12	3.5508E+09	2.8321E+13	2.9670	2.3434E+10
136.1121	02 - 04	1.2659E+10	5.2571E+11	1.5494	2.3298E+10
135.9624	10 - 08	2.3334E+09	7.1875E+12	1.0546	2.3262E+10
131.8496	10 - 10	2.3287E+09	7.1875E+12	1.0546	2.3216E+10
137.7713	06 - 06	4.2791E+09	5.6216E+11	0.6793	2.3192E+10
131.3350	08 - 08	3.8442E+09	2.0967E+13	4.6641	2.3179E+10
135.9507	08 - 06	5.1446E+09	9.5665E+11	1.8845	2.3094E+10
134.3209	10 - 10	2.3832E+09	2.3902E+14	3.1604	2.3021E+10
136.7103	10 - 10	2.2961E+09	5.6663E+12	1.5471	2.2822E+10
136.3211	10 - 12	2.2721E+09	3.3983E+13	0.0646	2.2705E+10
135.3097	08 - 10	5.0527E+09	9.5665E+11	1.8845	2.2681E+10
134.6890	10 - 08	3.3419E+09	1.0032E+12	1.8637	2.2678E+10
136.7746	08 - 06	2.9961E+09	7.8948E+11	0.9897	2.2639E+10
139.1297	08 - 08	2.9524E+09	6.1525E+11	0.3150	2.2503E+10
132.4896	10 - 10	2.2721E+09	2.6397E+12	0.3165	2.2454E+10
135.9019	02 - 04	1.3088E+10	3.6300E+11	1.1700	2.2349E+10
136.2976	06 - 06	3.7426E+09	2.7915E+12	1.3070	2.2201E+10
136.0049	04 - 06	6.1128E+09	3.6578E+11	1.3338	2.2200E+10
135.4687	10 - 10	2.1930E+09	3.3983E+13	0.0646	2.1914E+10
136.5109	08 - 08	2.7995E+09	1.1547E+12	0.6882	2.1852E+10
130.9182	08 - 08	3.1331E+09	8.3552E+12	2.7603	2.1803E+10
135.1806	04 - 06	5.9993E+09	3.6578E+11	1.3338	2.1788E+10
134.7690	08 - 08	2.8818E+09	6.6924E+11	0.0543	2.1787E+10
139.1273	10 - 08	2.2042E+09	2.6397E+12	0.3165	2.1783E+10
137.9183	06 - 06	3.8673E+09	4.3343E+11	0.0691	2.1741E+10
135.5652	08 - 06	2.7931E+09	1.5884E+12	1.0736	2.1734E+10
136.7804	06 - 08	3.6367E+09	1.0004E+13	0.4562	2.1720E+10
138.5941	10 - 10	2.1894E+09	2.8079E+12	0.8234	2.1584E+10
134.7668	10 - 08	3.1737E+09	1.0032E+12	1.8637	2.1536E+10
137.3432	10 - 08	2.1488E+09	2.9013E+13	0.5343	2.1460E+10
131.9718	06 - 06	3.5915E+09	5.5284E+12	0.5176	2.1397E+10
134.6030	10 - 10	3.2070E+09	2.8321E+13	2.9670	2.1165E+10
135.1567	08 - 10	3.7133E+09	5.7159E+12	3.0986	2.1129E+10
138.0841	04 - 02	5.5714E+09	9.1215E+11	1.1277	2.1124E+10
136.9872	08 - 06	2.7592E+09	5.8934E+11	0.1789	2.0907E+10
140.8638	06 - 06	9.7472E+09	2.5623E+13	5.3875	2.0860E+10
137.9523	06 - 08	3.5303E+09	2.2203E+12	0.1358	2.0835E+10

Table 7: Continued

λ	g_i - g_f	Ar	Aa	δE_{if}	Qd
135.1835	06 - 08	3.6667E+09	9.0421E+11	1.5801	2.0828E+10
134.0352	04 - 06	5.5386E+09	6.2520E+11	0.9033	2.0812E+10
134.2564	08 - 06	2.6136E+09	8.3050E+12	1.7172	2.0777E+10
130.3348	10 - 10	3.0249E+09	1.0032E+12	1.8637	2.0527E+10
135.5147	06 - 06	3.6133E+09	9.2648E+11	1.8325	2.0480E+10
131.5377	08 - 08	2.5811E+09	2.0829E+12	1.2532	2.0299E+10
135.5418	12 - 12	1.8068E+09	7.3999E+12	2.6167	2.0260E+10
131.2274	12 - 10	1.7267E+09	9.0028E+11	1.5005	2.0237E+10
137.8710	10 - 10	2.0291E+09	1.1367E+13	0.1823	2.0231E+10
135.7420	06 - 04	1.8795E+10	9.7695E+11	2.2007	2.0159E+10
145.7297	02 - 04	1.1743E+10	3.6300E+11	1.1700	2.0052E+10
142.1367	06 - 06	5.4401E+09	9.6578E+13	4.5993	1.9931E+10
133.2631	10 - 08	2.0497E+09	9.6906E+11	1.2602	1.9900E+10
137.3895	08 - 08	2.6306E+09	6.6924E+11	0.0543	1.9888E+10
131.8263	12 - 10	1.7212E+09	1.0479E+12	0.2270	1.9865E+10
136.6228	08 - 08	2.5618E+09	1.5396E+12	1.0103	1.9843E+10
133.6438	04 - 06	5.5552E+09	2.0205E+11	0.6407	1.9754E+10
134.5636	10 - 12	1.9709E+09	7.9710E+12	1.2525	1.9641E+10
137.0382	06 - 06	3.2873E+09	6.2448E+12	0.8154	1.9617E+10
136.0234	04 - 04	7.5682E+09	9.0307E+10	1.6088	1.9597E+10
135.5669	08 - 08	2.4593E+09	8.3050E+12	1.7172	1.9550E+10
134.2652	04 - 04	5.1349E+09	9.7498E+11	0.7059	1.9506E+10
134.1909	08 - 08	2.4481E+09	1.0518E+13	0.4506	1.9475E+10
132.9061	08 - 08	3.4208E+09	5.7159E+12	3.0986	1.9465E+10
136.4046	06 - 04	3.2577E+09	1.0004E+13	0.4562	1.9457E+10
137.5633	06 - 06	3.2537E+09	6.2448E+12	0.8154	1.9417E+10
137.1441	10 - 10	1.9986E+09	9.6906E+11	1.2602	1.9404E+10
137.4907	06 - 06	3.2529E+09	5.5284E+12	0.5176	1.9380E+10
132.9187	06 - 08	7.2058E+09	6.5867E+13	4.4791	1.9330E+10
136.0883	06 - 06	3.2857E+09	1.5408E+12	1.2780	1.9326E+10
142.3328	06 - 06	7.2037E+09	6.5867E+13	4.4791	1.9325E+10
136.8056	04 - 04	5.4475E+09	4.1005E+11	0.5673	1.9309E+10
132.2323	10 - 10	1.9301E+09	6.3533E+13	0.4986	1.9292E+10
132.4985	08 - 08	2.4593E+09	2.7467E+12	1.6308	1.9257E+10
134.6292	06 - 04	3.2208E+09	1.0004E+13	0.4562	1.9236E+10
132.7672	08 - 06	2.4392E+09	2.0829E+12	1.2532	1.9183E+10
129.0111	14 - 14	1.4251E+09	2.3417E+11	0.5835	1.9153E+10
137.5322	08 - 08	2.4555E+09	1.6962E+12	0.0138	1.9075E+10
136.3548	04 - 06	5.3253E+09	3.4764E+11	0.5440	1.9059E+10
129.3769	10 - 08	1.9989E+09	8.9232E+11	0.7396	1.9059E+10
135.2995	08 - 06	2.4076E+09	2.0829E+12	1.2532	1.8934E+10
131.4325	12 - 10	1.5854E+09	5.2908E+12	1.0691	1.8917E+10

Table 7: Continued

λ	g_i - g_f	Ar	Aa	δE_{if}	Qd
137.4546	10 - 08	1.8877E+09	3.3983E+13	0.0646	1.8863E+10
136.0306	06 - 06	3.1602E+09	6.2448E+12	0.8154	1.8859E+10
139.5206	12 - 12	1.5840E+09	1.1557E+12	0.0081	1.8791E+10
138.0190	02 - 02	1.1003E+10	3.6300E+11	1.1700	1.8789E+10
133.7832	04 - 04	5.7608E+09	2.4617E+11	1.0386	1.8772E+10
131.9880	10 - 10	1.8690E+09	3.4116E+13	0.6721	1.8668E+10
136.2249	06 - 06	3.2032E+09	1.1756E+12	0.6308	1.8661E+10
137.1262	06 - 08	3.1147E+09	6.2448E+12	0.8154	1.8587E+10
132.6339	10 - 10	1.8517E+09	6.3533E+13	0.4986	1.8508E+10
136.0331	02 - 04	1.0544E+10	4.0210E+11	0.2058	1.8490E+10
134.1132	08 - 10	2.4387E+09	7.8948E+11	0.9897	1.8427E+10
137.6816	08 - 08	2.3162E+09	1.0518E+13	0.4506	1.8426E+10
137.4512	08 - 08	2.3675E+09	1.6962E+12	0.0138	1.8391E+10
134.1708	06 - 08	3.1550E+09	1.1756E+12	0.6308	1.8380E+10
136.4017	02 - 02	1.0409E+10	4.0210E+11	0.2058	1.8253E+10
134.6688	04 - 02	4.7473E+09	9.7498E+11	0.7059	1.8034E+10
136.2348	10 - 10	2.6574E+09	1.0032E+12	1.8637	1.8033E+10
134.9017	06 - 08	3.0329E+09	5.1125E+12	1.7185	1.8032E+10
138.2135	04 - 04	5.0786E+09	4.1005E+11	0.5673	1.8001E+10
133.4528	06 - 06	3.0281E+09	2.7915E+12	1.3070	1.7962E+10
135.4153	06 - 08	3.0573E+09	2.3356E+12	1.4231	1.7942E+10
136.3541	10 - 08	1.8729E+09	8.9232E+11	0.7396	1.7857E+10
135.4737	12 - 14	1.4953E+09	5.2908E+12	1.0691	1.7842E+10
135.9723	06 - 04	3.1098E+09	8.4170E+11	0.2466	1.7793E+10
129.2671	10 - 12	1.7808E+09	1.1367E+13	0.1823	1.7756E+10
134.4670	04 - 04	5.0073E+09	4.1005E+11	0.5673	1.7748E+10
133.2730	08 - 08	2.2565E+09	2.0829E+12	1.2532	1.7746E+10
136.2216	08 - 06	2.2360E+09	3.0145E+12	1.1888	1.7696E+10
133.7888	08 - 06	2.2562E+09	1.5884E+12	1.0736	1.7556E+10
136.9519	02 - 04	9.1105E+09	1.1463E+12	0.9908	1.7523E+10
138.4857	10 - 12	1.7530E+09	3.4116E+13	0.6721	1.7509E+10
137.5820	10 - 12	1.8002E+09	9.6906E+11	1.2602	1.7478E+10
131.7078	04 - 06	4.5899E+09	9.7498E+11	0.7059	1.7436E+10
137.2231	08 - 10	2.1866E+09	8.3050E+12	1.7172	1.7382E+10
137.9430	04 - 06	4.8890E+09	4.1005E+11	0.5673	1.7329E+10
135.6981	06 - 04	2.9151E+09	2.7915E+12	1.3070	1.7292E+10
138.9296	08 - 10	2.1804E+09	3.3378E+12	0.0984	1.7275E+10
137.9654	04 - 04	5.1351E+09	2.7624E+11	0.3258	1.7170E+10
136.0706	06 - 04	3.1615E+09	5.6216E+11	0.6793	1.7135E+10
138.2144	12 - 10	1.4302E+09	5.2908E+12	1.0691	1.7065E+10
132.9366	08 - 06	2.7121E+09	2.3601E+13	2.8820	1.7058E+10
136.3411	06 - 06	2.8996E+09	1.5408E+12	1.2780	1.7055E+10

Table 7: Continued

λ	g_i - g_f	Ar	Aa	δE_{if}	Qd
138.2902	06 - 04	2.8623E+09	5.5284E+12	0.5176	1.7053E+10
133.0842	10 - 10	1.7066E+09	1.1367E+13	0.1823	1.7016E+10
137.9410	08 - 06	2.2405E+09	6.6924E+11	0.0543	1.6939E+10
132.9219	12 - 12	1.4538E+09	1.3256E+13	4.4196	1.6924E+10
136.7766	04 - 06	4.6515E+09	3.6578E+11	1.3338	1.6893E+10
137.4068	06 - 08	2.8921E+09	1.1756E+12	0.6308	1.6848E+10
136.0002	04 - 02	6.4861E+09	9.0307E+10	1.6088	1.6795E+10
132.2134	06 - 08	2.9590E+09	9.2648E+11	1.8325	1.6771E+10
131.5388	10 - 08	1.6777E+09	7.9710E+12	1.2525	1.6719E+10
134.6944	08 - 06	2.0990E+09	1.0518E+13	0.4506	1.6698E+10
136.9169	06 - 08	2.7935E+09	6.2448E+12	0.8154	1.6671E+10
131.3260	08 - 10	2.7463E+09	2.0967E+13	4.6641	1.6559E+10
135.8542	04 - 04	4.9252E+09	2.7624E+11	0.3258	1.6468E+10
136.7806	12 - 10	1.3982E+09	9.0028E+11	1.5005	1.6387E+10
136.4047	04 - 04	8.4876E+09	3.5775E+10	1.7569	1.6386E+10
134.2051	10 - 10	2.5017E+09	1.9286E+13	3.7491	1.6344E+10
136.7009	04 - 06	5.0116E+09	2.4617E+11	1.0386	1.6331E+10
136.7652	04 - 06	4.8721E+09	2.7624E+11	0.3258	1.6291E+10
137.1511	06 - 06	3.2011E+09	2.5658E+11	0.0161	1.6185E+10
131.7758	10 - 10	1.6394E+09	2.8079E+12	0.8234	1.6162E+10
130.9679	06 - 08	6.0015E+09	6.5867E+13	4.4791	1.6100E+10
138.7297	12 - 10	1.3858E+09	1.0479E+12	0.2270	1.5994E+10
136.3004	04 - 04	4.2531E+09	6.2520E+11	0.9033	1.5982E+10
134.3110	10 - 08	1.5993E+09	2.9013E+13	0.5343	1.5972E+10
137.6777	08 - 08	2.0863E+09	6.1525E+11	0.3150	1.5902E+10
134.5578	04 - 06	4.4430E+09	3.4764E+11	0.5440	1.5901E+10
131.0137	10 - 12	2.4338E+09	1.9286E+13	3.7491	1.5900E+10
137.5557	08 - 10	2.1017E+09	7.8948E+11	0.9897	1.5881E+10
145.2220	06 - 06	2.6346E+09	5.1125E+12	1.7185	1.5664E+10
137.4783	06 - 06	2.6130E+09	2.3797E+13	0.8711	1.5662E+10
132.5104	06 - 06	2.6462E+09	2.2203E+12	0.1358	1.5617E+10
130.9952	10 - 08	2.1030E+09	9.5350E+12	2.7046	1.5493E+10
137.6084	10 - 08	1.5479E+09	6.3533E+13	0.4986	1.5472E+10
137.4621	06 - 08	2.5895E+09	1.0004E+13	0.4562	1.5466E+10
136.7966	10 - 08	1.5451E+09	6.3533E+13	0.4986	1.5444E+10
134.5446	04 - 06	4.0490E+09	9.0187E+11	1.8220	1.5413E+10
136.5772	08 - 06	1.9343E+09	1.0518E+13	0.4506	1.5388E+10
133.7393	10 - 08	2.3264E+09	2.8321E+13	2.9670	1.5353E+10
134.8252	10 - 08	1.5377E+09	1.1367E+13	0.1823	1.5332E+10
132.6527	04 - 06	4.2167E+09	3.6578E+11	1.3338	1.5314E+10
135.2549	06 - 06	2.7104E+09	4.3343E+11	0.0691	1.5237E+10
134.3860	10 - 08	1.5415E+09	2.6397E+12	0.3165	1.5234E+10

Table 7: Continued

λ	g_i - g_f	Ar	Aa	δE_{if}	Qd
135.6386	06 - 06	2.6807E+09	9.0421E+11	1.5801	1.5227E+10
138.7278	04 - 04	4.5762E+09	2.5838E+11	0.2348	1.5210E+10
137.4711	08 - 08	1.9313E+09	1.4734E+12	0.5885	1.5175E+10
132.9354	10 - 08	1.6260E+09	9.2625E+13	3.5276	1.5170E+10
133.0517	04 - 02	3.9791E+09	9.7498E+11	0.7059	1.5116E+10
134.0130	10 - 08	1.5839E+09	8.9232E+11	0.7396	1.5102E+10
136.9915	10 - 08	1.5254E+09	2.6397E+12	0.3165	1.5075E+10
130.9162	10 - 12	1.5511E+09	9.6906E+11	1.2602	1.5059E+10
136.5621	08 - 08	1.8982E+09	3.0145E+12	1.1888	1.5023E+10
138.0096	08 - 08	1.8957E+09	3.3378E+12	0.0984	1.5019E+10
131.6617	08 - 10	1.8932E+09	3.0145E+12	1.1888	1.4983E+10
132.7020	08 - 10	1.8686E+09	1.0518E+13	0.4506	1.4865E+10
134.1456	02 - 04	8.4629E+09	4.0210E+11	0.2058	1.4840E+10
134.6979	08 - 06	1.8654E+09	8.3050E+12	1.7172	1.4829E+10
135.9839	04 - 06	4.1408E+09	3.4764E+11	0.5440	1.4820E+10
135.6070	02 - 04	7.6757E+09	1.1463E+12	0.9908	1.4763E+10
130.6579	08 - 10	8.2631E+09	5.5407E+13	6.2572	1.4670E+10
131.8370	08 - 08	1.8414E+09	1.0518E+13	0.4506	1.4649E+10
134.2024	12 - 12	1.2424E+09	9.0028E+11	1.5005	1.4561E+10
136.7889	02 - 04	7.5677E+09	6.7304E+11	0.5784	1.4509E+10
135.8547	06 - 06	2.4895E+09	1.1756E+12	0.6308	1.4503E+10
136.8409	04 - 04	4.0503E+09	3.4764E+11	0.5440	1.4496E+10
135.5778	10 - 08	1.4931E+09	9.6906E+11	1.2602	1.4496E+10
133.4256	12 - 10	1.2168E+09	4.8785E+12	1.4661	1.4484E+10
135.6566	10 - 08	1.4843E+09	9.6906E+11	1.2602	1.4411E+10
133.1261	06 - 08	1.0259E+10	1.3821E+13	4.3337	1.4409E+10
137.6754	10 - 08	1.4545E+09	2.6397E+12	0.3165	1.4374E+10
131.6439	08 - 08	1.8284E+09	1.4734E+12	0.5885	1.4366E+10
134.5293	06 - 06	2.5267E+09	9.2648E+11	1.8325	1.4321E+10
130.9693	08 - 08	1.8386E+09	1.5884E+12	1.0736	1.4307E+10
138.5932	08 - 10	1.8764E+09	6.1525E+11	0.3150	1.4302E+10
137.7577	08 - 06	1.8321E+09	1.1547E+12	0.6882	1.4301E+10
138.2521	10 - 12	1.4375E+09	2.8079E+12	0.8234	1.4171E+10
133.5404	08 - 10	2.4814E+09	5.7159E+12	3.0986	1.4119E+10
134.5238	04 - 06	3.9543E+09	4.1005E+11	0.5673	1.4016E+10
137.2510	08 - 10	1.7796E+09	1.4734E+12	0.5885	1.3983E+10
134.8296	10 - 10	2.4889E+09	2.8667E+12	2.2108	1.3963E+10
133.6769	10 - 12	2.0575E+09	1.0032E+12	1.8637	1.3962E+10
135.6904	06 - 04	2.4587E+09	9.2648E+11	1.8325	1.3935E+10
133.8522	02 - 04	7.2284E+09	1.1463E+12	0.9908	1.3903E+10
133.4461	02 - 02	7.5534E+09	5.2571E+11	1.5494	1.3901E+10
138.2417	08 - 06	1.1263E+10	3.5017E+13	7.0570	1.3883E+10

Table 7: Continued

λ	g_i - g_f	Ar	Aa	δE_{if}	Qd
134.0254	06 - 04	2.3145E+09	2.3797E+13	0.8711	1.3873E+10
134.7771	10 - 10	1.3836E+09	2.9013E+13	0.5343	1.3818E+10
136.4371	02 - 02	1.1775E+10	5.9710E+10	1.3170	1.3817E+10
140.5049	06 - 04	9.8035E+09	1.3821E+13	4.3337	1.3769E+10
132.1516	06 - 08	2.3064E+09	6.2448E+12	0.8154	1.3764E+10
135.0323	04 - 02	3.6267E+09	9.1215E+11	1.1277	1.3750E+10
133.6227	08 - 06	1.7336E+09	3.0145E+12	1.1888	1.3720E+10
131.4527	10 - 10	1.3736E+09	7.1875E+12	1.0546	1.3694E+10
136.3067	06 - 06	2.3490E+09	1.1756E+12	0.6308	1.3684E+10
131.9855	06 - 04	2.2980E+09	5.1125E+12	1.7185	1.3663E+10
136.4604	02 - 04	1.1605E+10	5.9710E+10	1.3170	1.3618E+10
134.9797	06 - 08	2.2801E+09	5.1125E+12	1.7185	1.3556E+10
135.5237	08 - 08	3.0189E+09	9.5665E+11	1.8845	1.3552E+10
134.1213	10 - 08	1.3550E+09	6.3533E+13	0.4986	1.3543E+10
135.2202	06 - 06	2.2826E+09	2.7915E+12	1.3070	1.3540E+10
130.8101	08 - 08	1.7052E+09	3.0145E+12	1.1888	1.3495E+10
136.3782	08 - 06	1.7137E+09	2.0829E+12	1.2532	1.3477E+10
132.3654	08 - 10	1.7192E+09	1.1547E+12	0.6882	1.3419E+10
132.3881	10 - 10	1.3384E+09	3.4116E+13	0.6721	1.3368E+10
135.9157	08 - 10	1.6716E+09	1.9947E+13	1.4760	1.3362E+10
137.4293	04 - 06	3.5530E+09	6.2520E+11	0.9033	1.3351E+10
137.5538	10 - 08	1.3348E+09	2.9013E+13	0.5343	1.3331E+10
134.5497	06 - 06	2.6353E+09	2.5658E+11	0.0161	1.3324E+10
135.6555	04 - 02	3.5037E+09	9.7498E+11	0.7059	1.3310E+10
134.0089	10 - 08	7.7881E+09	2.4189E+12	3.7202	1.3278E+10
134.6873	08 - 08	2.1982E+09	3.9568E+12	2.3144	1.3272E+10
132.1696	10 - 08	1.9504E+09	1.0032E+12	1.8637	1.3235E+10
129.5690	12 - 10	1.1458E+09	1.0479E+12	0.2270	1.3224E+10
132.3536	06 - 06	2.3098E+09	8.4170E+11	0.2466	1.3216E+10
130.9956	10 - 08	1.3247E+09	7.1875E+12	1.0546	1.3206E+10
136.9698	06 - 06	2.2364E+09	2.2203E+12	0.1358	1.3199E+10
138.0774	08 - 08	1.7424E+09	6.6924E+11	0.0543	1.3173E+10
131.4133	06 - 04	2.5796E+09	2.5658E+11	0.0161	1.3042E+10
136.8001	06 - 08	2.2982E+09	9.2648E+11	1.8325	1.3026E+10
135.1305	02 - 04	7.2595E+09	2.3789E+11	1.6908	1.2998E+10
132.3353	12 - 12	5.8791E+09	5.0302E+11	4.8331	1.2959E+10
139.5978	06 - 08	2.5586E+09	2.5658E+11	0.0161	1.2936E+10
137.7307	04 - 06	3.3838E+09	9.7498E+11	0.7059	1.2854E+10
140.5066	08 - 06	1.1344E+10	3.8089E+12	5.6113	1.2829E+10
135.3128	08 - 06	2.1179E+09	3.9568E+12	2.3144	1.2788E+10
137.0682	06 - 04	2.5250E+09	2.5658E+11	0.0161	1.2766E+10
137.2179	06 - 04	2.1349E+09	6.2448E+12	0.8154	1.2740E+10
131.7450	06 - 06	2.3484E+09	5.6216E+11	0.6793	1.2728E+10

Table 7: Continued

λ	g_i - g_f	Ar	Aa	δE_{if}	Qd
134.3196	10 - 08	1.7206E+09	9.5350E+12	2.7046	1.2676E+10
137.3270	06 - 06	2.1192E+09	1.0004E+13	0.4562	1.2657E+10
138.8140	06 - 08	2.1202E+09	5.5284E+12	0.5176	1.2632E+10
133.7108	04 - 06	3.3303E+09	9.1215E+11	1.1277	1.2627E+10
138.5494	08 - 08	1.6132E+09	1.1547E+12	0.6882	1.2592E+10
131.6144	06 - 08	2.1990E+09	8.4170E+11	0.2466	1.2582E+10
133.7320	08 - 10	1.5977E+09	2.0829E+12	1.2532	1.2565E+10
131.7010	10 - 10	1.2655E+09	2.6397E+12	0.3165	1.2506E+10
136.5624	08 - 06	1.5631E+09	1.9947E+13	1.4760	1.2494E+10
129.1178	08 - 10	1.7809E+09	8.3552E+12	2.7603	1.2393E+10
136.5243	06 - 08	2.2703E+09	5.6216E+11	0.6793	1.2304E+10
138.0516	10 - 10	1.2128E+09	3.3983E+13	0.0646	1.2119E+10
133.3897	08 - 08	1.7408E+09	8.3552E+12	2.7603	1.2114E+10
137.3306	02 - 02	6.7329E+09	2.3695E+11	0.7257	1.2101E+10
133.5300	08 - 06	1.5160E+09	2.0829E+12	1.2532	1.1922E+10
134.4296	08 - 06	1.5012E+09	3.3378E+12	0.0984	1.1893E+10
132.4719	08 - 08	1.5133E+09	1.4734E+12	0.5885	1.1890E+10
140.6734	06 - 06	4.4286E+09	6.5867E+13	4.4791	1.1880E+10
136.5955	06 - 06	2.0125E+09	2.2203E+12	0.1358	1.1877E+10
136.4060	06 - 06	2.0901E+09	9.0421E+11	1.5801	1.1872E+10
131.1776	10 - 10	1.1910E+09	7.9710E+12	1.2525	1.1869E+10
133.2904	08 - 08	1.5130E+09	1.6962E+12	0.0138	1.1753E+10
136.9736	06 - 04	1.9660E+09	1.0004E+13	0.4562	1.1742E+10
136.2405	06 - 08	1.9664E+09	6.2448E+12	0.8154	1.1735E+10
136.2285	10 - 08	1.1859E+09	2.8079E+12	0.8234	1.1691E+10
136.2881	08 - 06	1.4862E+09	1.4734E+12	0.5885	1.1678E+10
139.4856	08 - 06	6.5666E+09	5.5407E+13	6.2572	1.1658E+10
134.8988	06 - 06	2.0504E+09	9.0421E+11	1.5801	1.1647E+10
129.5023	12 - 12	9.8067E+08	1.1557E+12	0.0081	1.1634E+10
136.6991	08 - 06	1.5191E+09	6.1525E+11	0.3150	1.1578E+10
131.6313	06 - 04	1.9597E+09	2.2203E+12	0.1358	1.1566E+10
136.3942	08 - 06	1.4858E+09	1.5884E+12	1.0736	1.1561E+10
133.2668	06 - 04	1.9349E+09	6.2448E+12	0.8154	1.1547E+10
133.7726	10 - 08	1.2099E+09	8.9232E+11	0.7396	1.1536E+10
134.9154	08 - 08	2.0256E+09	5.7159E+12	3.0986	1.1526E+10
134.7409	10 - 12	1.1922E+09	2.3902E+14	3.1604	1.1516E+10
132.3593	12 - 10	9.7639E+08	1.8705E+12	0.6925	1.1483E+10
132.9817	08 - 08	2.0143E+09	5.7159E+12	3.0986	1.1462E+10
136.0448	08 - 06	1.4307E+09	1.9947E+13	1.4760	1.1436E+10
136.1776	06 - 08	1.9274E+09	2.7915E+12	1.3070	1.1433E+10
139.1741	08 - 10	1.4320E+09	1.0518E+13	0.4506	1.1392E+10
134.3218	04 - 06	2.9845E+09	9.7498E+11	0.7059	1.1337E+10

Table 7: Continued

λ	g_i - g_f	Ar	Aa	δE_{if}	Qd
138.0547	06 - 08	2.0159E+09	4.3343E+11	0.0691	1.1333E+10
137.5844	06 - 06	1.8961E+09	1.0004E+13	0.4562	1.1324E+10
132.3309	08 - 08	1.4507E+09	1.1547E+12	0.6882	1.1324E+10
134.0190	10 - 10	1.1293E+09	7.1875E+12	1.0546	1.1258E+10
136.4866	06 - 06	1.8805E+09	1.0004E+13	0.4562	1.1231E+10
138.1386	12 - 10	9.4389E+08	1.1557E+12	0.0081	1.1197E+10
137.0610	04 - 02	2.9693E+09	6.2520E+11	0.9033	1.1158E+10
131.3119	08 - 06	1.4736E+09	7.8948E+11	0.9897	1.1135E+10
131.4471	10 - 12	2.2589E+10	2.2703E+12	5.4662	1.1123E+10
136.2099	04 - 06	3.1278E+09	2.0205E+11	0.6407	1.1122E+10
132.9459	04 - 06	2.9279E+09	9.1215E+11	1.1277	1.1101E+10
135.3961	06 - 08	1.9570E+09	9.2648E+11	1.8325	1.1092E+10
136.4446	06 - 08	2.0376E+09	5.6216E+11	0.6793	1.1043E+10
135.8719	06 - 06	1.8814E+09	2.3356E+12	1.4231	1.1041E+10
130.1645	04 - 06	2.8755E+09	9.0187E+11	1.8220	1.0946E+10
139.8043	06 - 06	1.5962E+10	2.9651E+13	6.0546	1.0938E+10
133.8803	08 - 06	1.4042E+09	1.5396E+12	1.0103	1.0877E+10
134.8531	10 - 12	1.0899E+09	7.1875E+12	1.0546	1.0866E+10
134.3630	10 - 08	1.0832E+09	6.3533E+13	0.4986	1.0827E+10
137.1547	08 - 10	1.3761E+09	2.0829E+12	1.2532	1.0822E+10
137.1780	06 - 08	1.8875E+09	8.4170E+11	0.2466	1.0799E+10
132.3436	06 - 08	1.9824E+09	5.6216E+11	0.6793	1.0744E+10
130.1221	12 - 14	4.8715E+09	5.0302E+11	4.8331	1.0738E+10
137.9788	04 - 06	2.9975E+09	3.4764E+11	0.5440	1.0728E+10
133.9101	06 - 06	1.7951E+09	1.0004E+13	0.4562	1.0721E+10
132.9367	06 - 06	1.8669E+09	8.6631E+11	1.1342	1.0706E+10
130.6913	10 - 08	1.5749E+09	1.0032E+12	1.8637	1.0687E+10
133.1272	08 - 08	1.3485E+09	3.0145E+12	1.1888	1.0672E+10
136.7828	06 - 06	1.7801E+09	6.2448E+12	0.8154	1.0623E+10
135.3008	06 - 06	1.7822E+09	2.7915E+12	1.3070	1.0572E+10
137.1338	10 - 08	1.0559E+09	3.4116E+13	0.6721	1.0547E+10
133.2342	06 - 08	9.4324E+09	3.2940E+12	4.2582	1.0542E+10
134.4109	08 - 10	1.8431E+09	5.7159E+12	3.0986	1.0487E+10
138.0626	10 - 08	1.0531E+09	7.8055E+12	1.0038	1.0472E+10
130.5849	12 - 12	8.9255E+08	9.0028E+11	1.5005	1.0461E+10
134.5395	06 - 04	1.7492E+09	5.5284E+12	0.5176	1.0421E+10
135.2117	08 - 06	1.3140E+09	3.3378E+12	0.0984	1.0410E+10
131.6602	02 - 02	5.7566E+09	2.3789E+11	1.6908	1.0307E+10
137.8861	08 - 08	1.3582E+09	5.8934E+11	0.1789	1.0291E+10
132.3658	08 - 06	1.3225E+09	1.6962E+12	0.0138	1.0273E+10

Table 8: Atomic data of λ, Ar, Aa, δE_{if},and Qd for the transition from the states of $4d^7 5p^1 5d$ to $4d^8 5d$ with the initial states $4d^8(i_0 = 6)$ of the Xe^{10+} ions

λ	g_i - g_f	Ar	Aa	δE_{if}	Qd
129.2678	12 - 14	2.9345E+09	3.4957E+12	0.0039	2.2273E+10
131.4471	10 - 12	2.2589E+10	3.2288E+13	0.0072	1.5819E+11
131.7562	10 - 10	1.2332E+10	3.2288E+13	0.0072	8.6361E+10
131.6799	08 - 10	5.0472E+09	4.5187E+13	0.0618	1.1050E+10
140.5066	08 - 06	1.1344E+10	1.0887E+13	0.1524	3.6670E+10
131.0252	10 - 08	3.2951E+09	6.9024E+12	0.3681	1.4263E+10
129.9246	10 - 08	2.9608E+09	6.9024E+12	0.3681	1.2816E+10
139.6622	08 - 06	2.6594E+10	9.5030E+13	0.6858	1.2157E+11
137.8916	08 - 06	2.0303E+10	4.9312E+13	0.7982	3.2079E+10
130.6579	08 - 10	8.2631E+09	4.9312E+13	0.7982	1.3056E+10
139.4856	08 - 06	6.5666E+09	4.9312E+13	0.7982	1.0375E+10
141.0423	06 - 04	6.4690E+09	1.1087E+14	1.4667	1.8987E+10
129.4505	12 - 10	9.2336E+08	3.0300E+14	1.6833	1.0846E+10
140.4840	06 - 04	1.5284E+10	3.6303E+13	1.8161	1.3127E+10
137.9064	06 - 06	1.4612E+10	3.6303E+13	1.8161	1.2550E+10
125.0792	10 - 12	4.8776E+09	5.1960E+13	2.7802	4.0930E+10
126.7216	10 - 08	1.4548E+09	5.1960E+13	2.7802	1.2208E+10
134.8262	08 - 06	4.0501E+09	1.0635E+14	2.8425	1.2812E+10
138.0668	06 - 04	4.7002E+10	1.8624E+14	3.3613	1.5073E+11
133.7069	06 - 04	4.6130E+09	1.8624E+14	3.3613	1.4793E+10
124.7099	12 - 14	3.7680E+09	8.8663E+13	3.5093	3.9402E+10
126.7413	12 - 12	1.0078E+09	8.8663E+13	3.5093	1.0539E+10
133.4823	08 - 06	8.0930E+09	2.9727E+14	3.7684	5.3682E+10
125.2161	08 - 10	4.4214E+09	4.0866E+13	4.4132	1.3518E+10
136.1220	06 - 04	1.5215E+10	4.4014E+13	4.6442	3.0909E+10
124.5241	10 - 12	3.4067E+09	4.7410E+13	5.2512	2.6390E+10

Table 9: Atomic data of λ, Ar, Aa, δE_{if},and Qd for the transition from the states of $4d^75p^15d$ to $4d^85d$ with the initial states $4d^8(i_0 = 4)$ of the Xe^{10+} ions

λ	g_i - g_f	Ar	Aa	δE_{if}	Qd
139.8574	2 - 4	1.7713E+10	4.0592E+13	0.2400	2.4785E+10
137.4607	2 - 4	1.8805E+10	1.5279E+13	1.7857	1.2236E+10
141.0755	4 - 4	2.6465E+10	4.2666E+13	2.4028	1.4056E+10
136.9051	4 - 6	2.6167E+10	4.2666E+13	2.4028	1.3898E+10
139.1721	4 - 4	4.3806E+10	5.6928E+13	3.6048	3.0702E+10
137.1776	4 - 4	2.9214E+10	1.7962E+13	4.9001	1.2150E+10

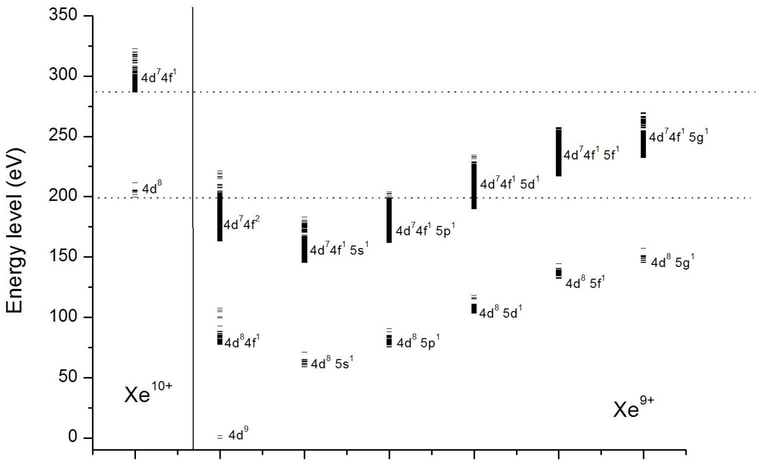

Figure 1: Energy level diagram of $4p^6 4d^7 4f^1, 4p^6 4d^8$ of the Xe^{10+} ions and $4p^6 4d^7 4f^2, 4p^6 4d^7 4f^1 5l, 4p^6 4d^8 4f^1, 4p^6 4d^8 5l$, and $4p^6 4d^9$ of the Xe^{9+} ions.

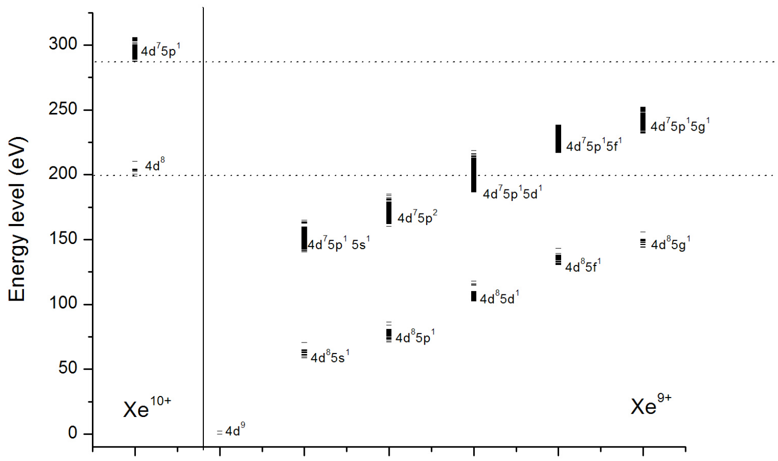

Figure 2: Energy level diagram of $4p^6 4d^7 5p^1, 4p^6 4d^8$ of the Xe^{10+} ions and $4p^6 4d^7 5p^1 5l, 4p^6 4d^8 5l$, and $4p^6 4d^9$ of the Xe^{9+} ions.

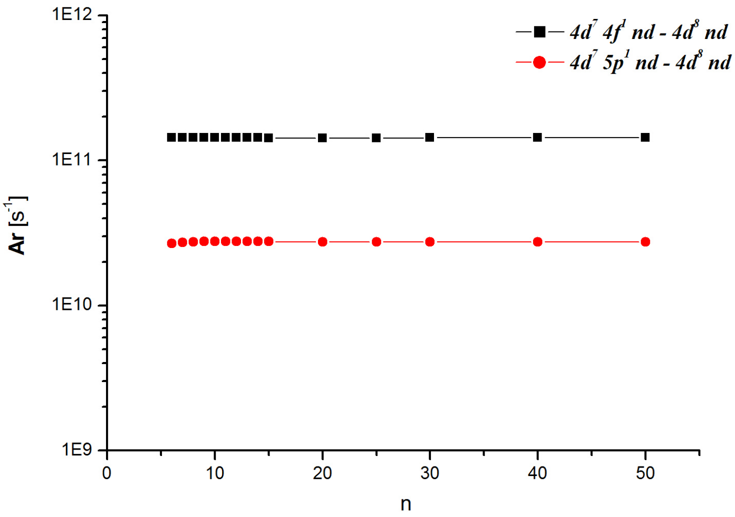

(a)

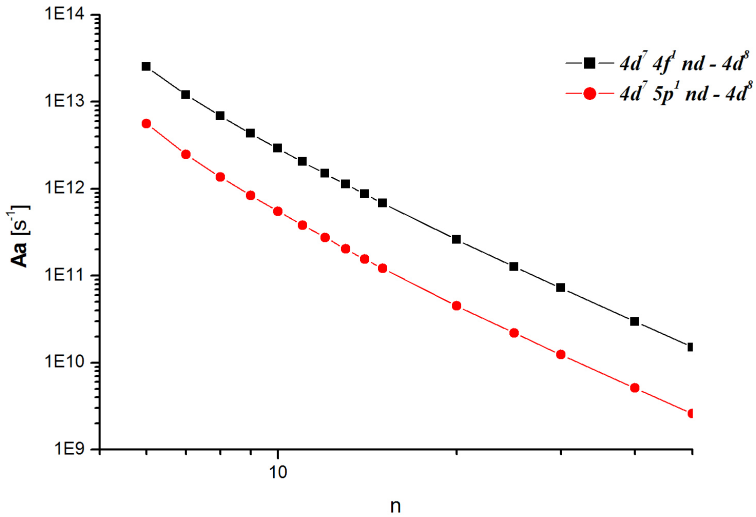

(b)

Figure 3: (a) The average $\bar{A}r[\equiv \Sigma g_i A_{ij}/\Sigma g_i]$ values of the $4d^7 4f^1 nd \rightarrow 4d^8 nd$ and $4d^7 5p^1 nd \rightarrow 4d^8 nd$ calculated with different n values at $l = 2$. (b) The average $\bar{A}a[\equiv \Sigma g_i Aa_{i,i_0}/\Sigma g_i]$ values of the $4d^7 4f^1 nd \rightarrow 4d^8 + e$ and $4d^7 5p^1 nd \rightarrow 4d^8 + e$ calculated with different n values at $l = 2$.

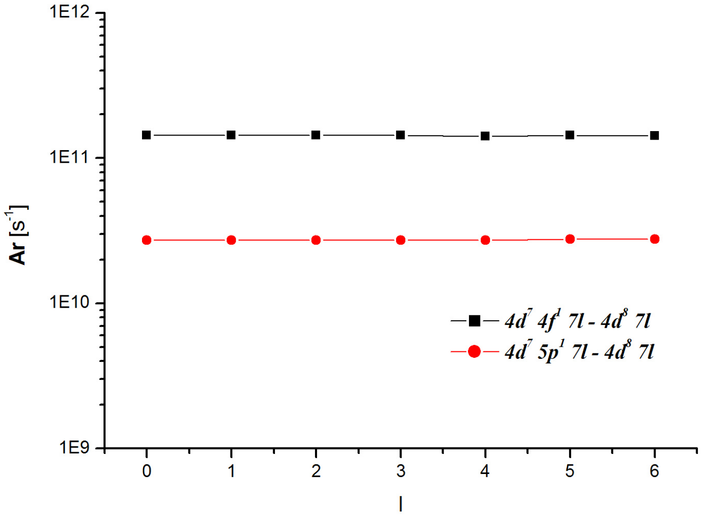

(a)

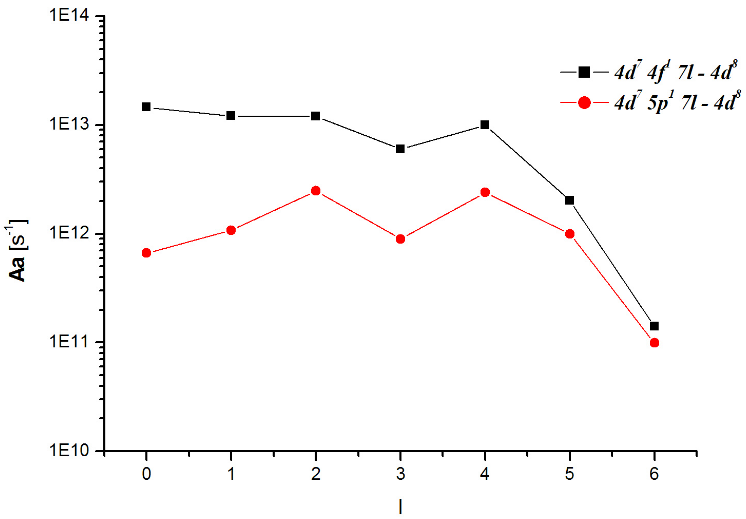

(b)

Figure 4: (a) The average $\bar{A}r$ of transition of $4d^7 4f^1 7l \rightarrow 4d^8 7l$ and $4d^7 5p^1 7l \rightarrow 4d^8 7l$ calculated with different l values at $n = 7$. (b) The average $\bar{A}a$ of transition of $4d^7 4f^1 7l \rightarrow 4d^8 + e$ and $4d^7 5p^1 7l \rightarrow 4d^8 + e$ calculated with different l values at $n = 7$.

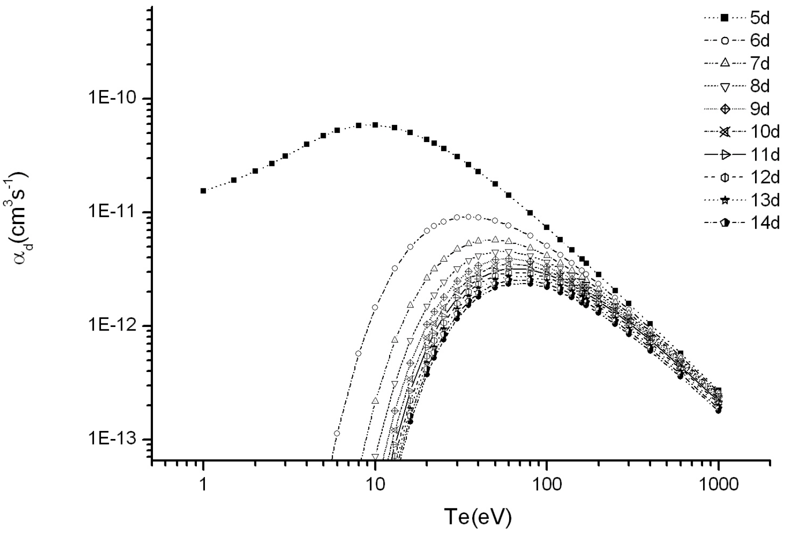

Figure 5: Dielectronic recombination rate coefficient for $4d^8 - 4d^7 4f^1 nd - 4^8 nd$ calculated with different n values as function of the plasma temperature.

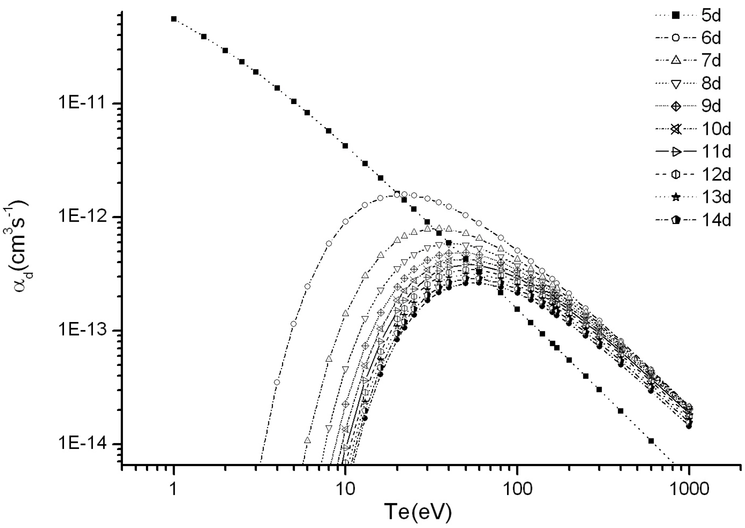

Figure 6: Dielectronic recombination rate coefficient for $4d^8 - 4d^7 5p^1 nd - 4d^8 nd$ calculated with different n values as function of the plasma temperature.

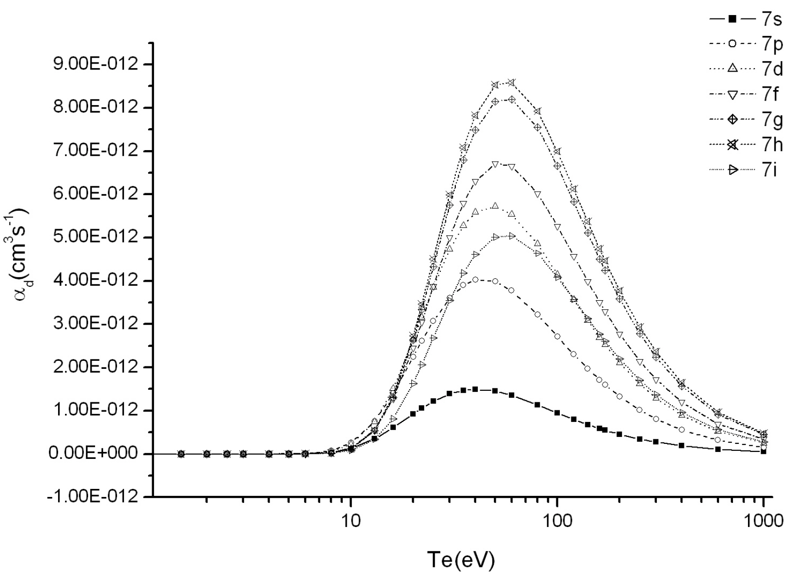

Figure 7: Dielectronic recombination rate coefficient for $4d^8 - 4d^7 4f^1 7l - 4d^8 7l$ calculated with different l values as function of the plasma temperature.

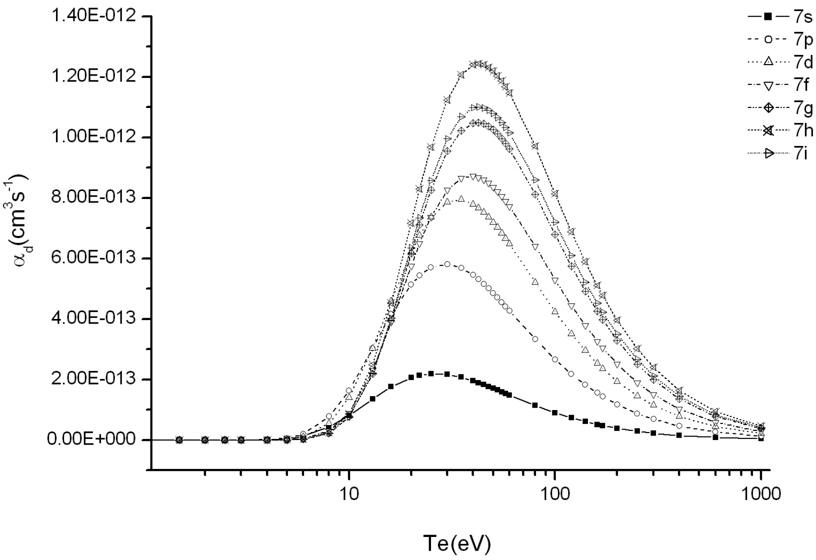

Figure 8: Dielectronic recombination rate coefficient for $4d^8 - 4d^7 5p^1 7l - 4d^8 7l$ calculated with different l values as function of the plasma temperature.

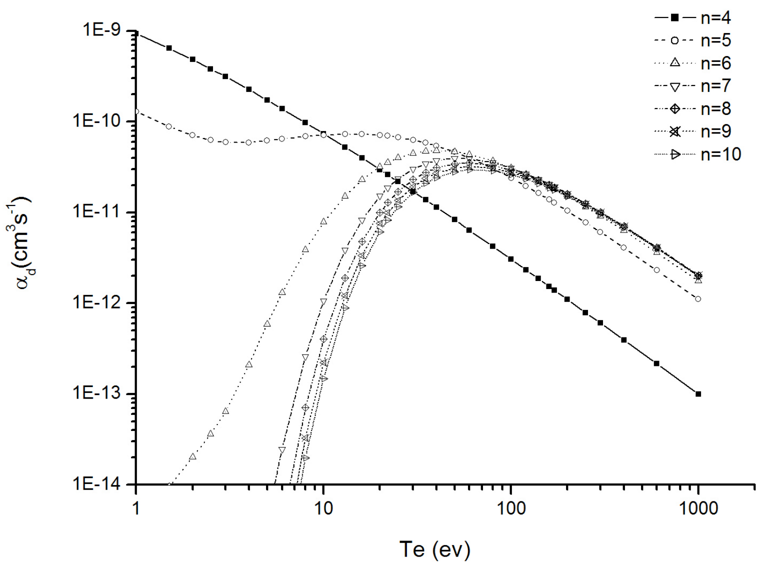

Figure 9: Dielectronic recombination rate coefficient for $4d^8 - 4d^7 4f^1 nl - 4d^8 nl$ calculated with different n values as function of the plasma temperature.

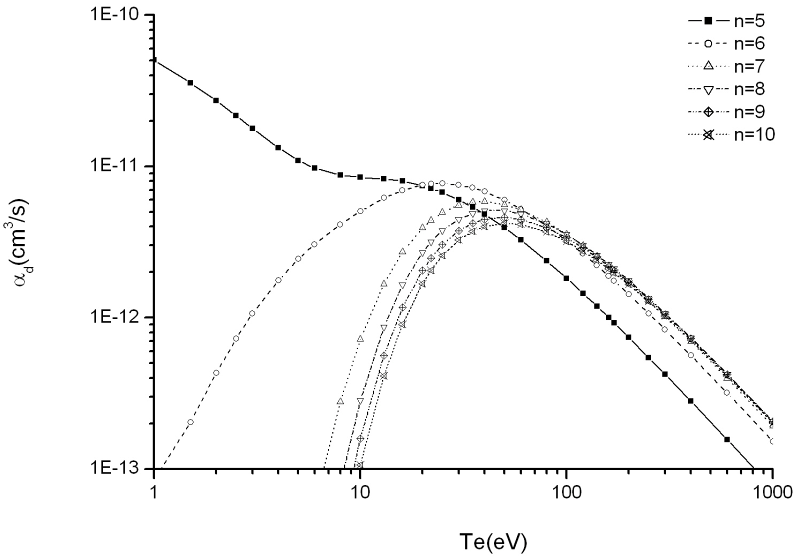

Figure 10: Dielectronic recombination rate coefficient for $4d^8 - 4d^7 5p^1 nl - 4d^8 nl$ calculated with different n values as function of the plasma temperature.

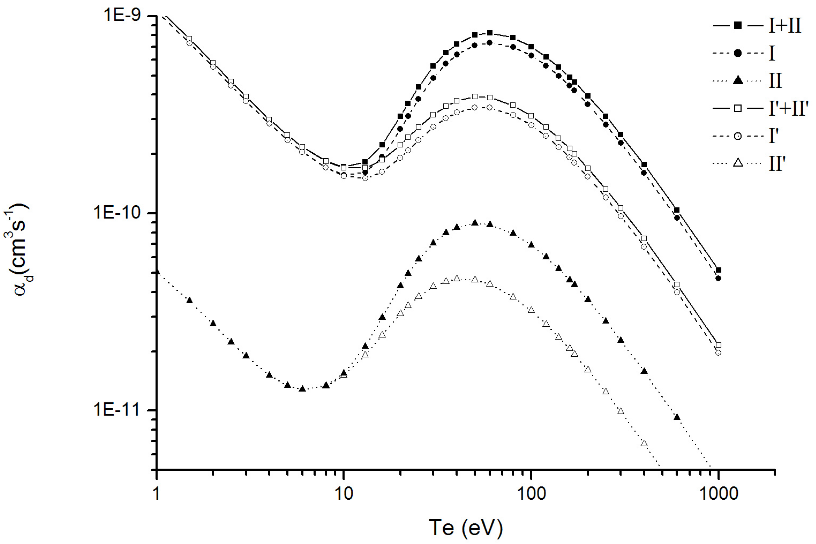

Figure 11: Total dielectronic recombination rate coefficient obtained by the summation of the each dielectronic recombination rate coefficient for these autoionizing states of I, II, I', and II'[I : $4d^8 - 4d^7 4f^1 nl - 4d^8 nl$ $(n = 4 - 100, l = 0 - 6)$, II : $4d^8 - 4d^7 5p^1 nl - 4d^8 nl$ $(n = 5 - 100, l = 0 - 6)$, I' : $4d^8 - 4d^7 4f^1 nl - 4d^8 nl$ $(n = 5 - 15, l = n - 1)$, II' : $4d^8 - 4d^7 5p^1 nl - 4d^8 nl$ $(n = 5 - 15, l = n - 1)$].

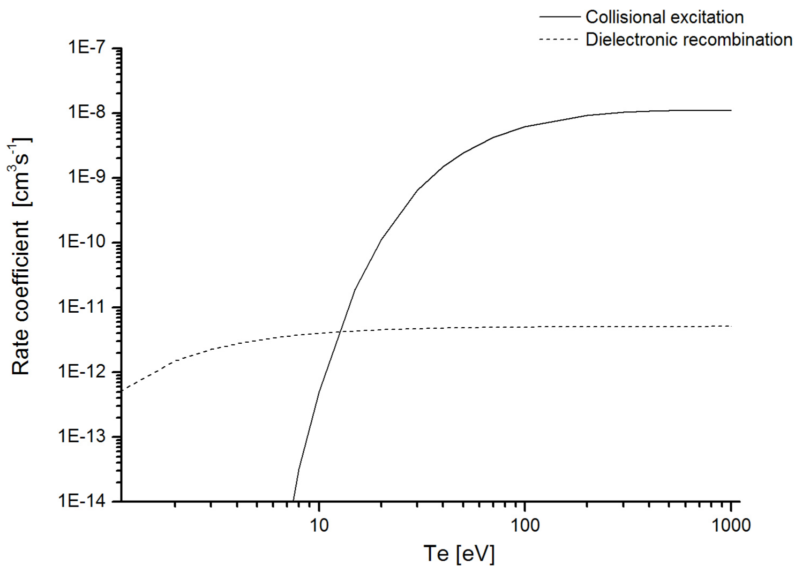

Figure 12: Comparison of rate coefficient of satellite line for $[4d^8(2J=8) \rightarrow 4d^7 4f^2(2J=15) \rightarrow 4d^8 4f^1(2J=13) : 112.3256\dot{A}]$ (dashed line) and rate coefficient of collisional excitation line for the $[4d^8(2J=8) \rightarrow 4d^7 4f^1(2J=8) : 111.572\dot{A}]$ of Xe^{10+} (solid line) ions as function of the plasma temperature.

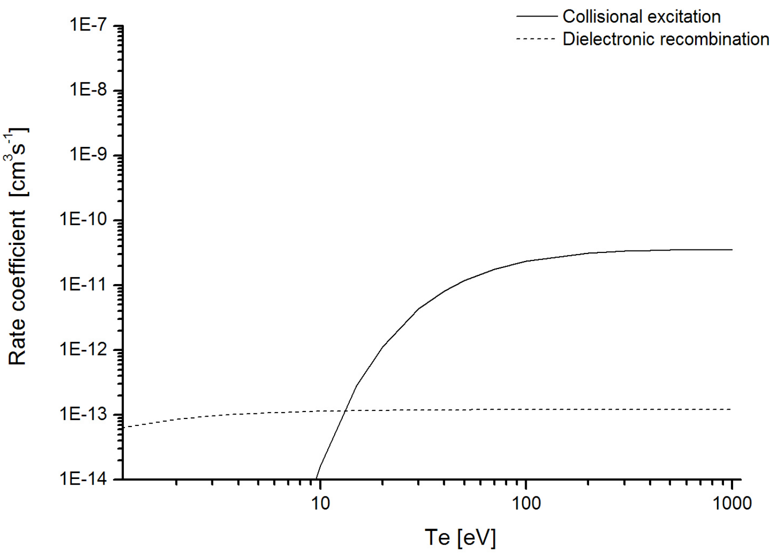

Figure 13: Comparison of rate coefficient of satellite line for $[4d^8(2J = 8) \rightarrow 4d^7 5p^1 5d^1(2J = 11) \rightarrow 4d^8 5d^1(2J = 13) : 136.0335\dot{A}]$(dashed line) and rate coefficient of collisional excitation line for the $[4d^8(2J = 8) \rightarrow 4d^7 5p^1(2J = 10) : 135.859\dot{A}]$ of Xe^{10+} (solid line) ions as function of the plasma temperature.

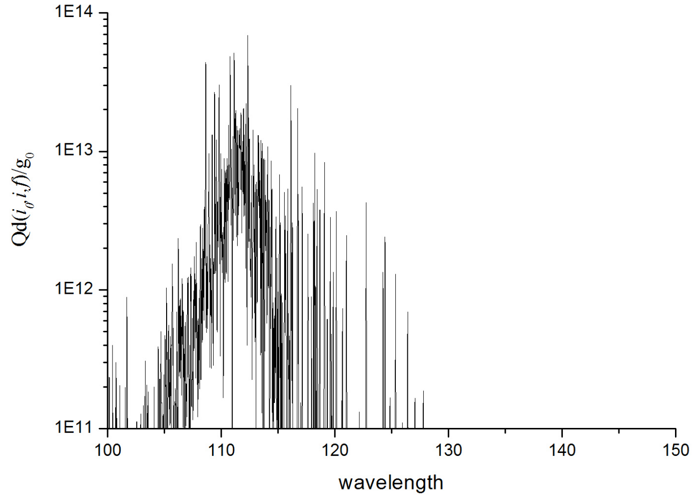

(a)

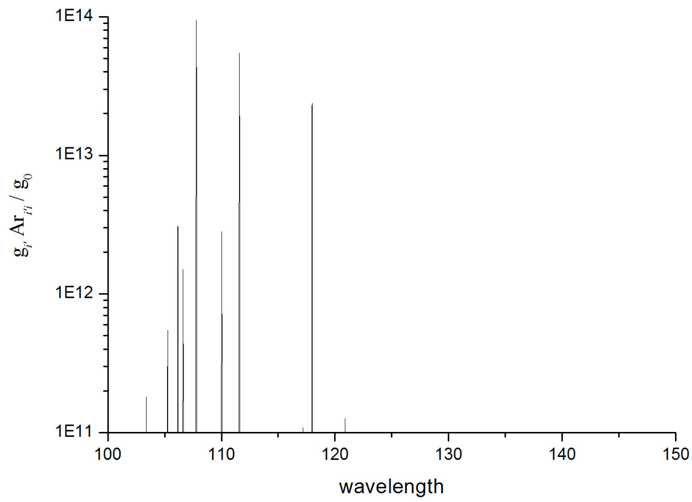

(b)

Figure 14: Satellite lines produced by dielectronic recombination ($4d^8\ ^3F_4 \rightarrow 4d^7 4f^2 \rightarrow 4d^8 4f^1$) of Xe^{9+} ion and radiative line that is obtained by radiative decay ($4d^7 4f^1 \rightarrow 4d^8\ ^3F_4$) of Xe^{10+} ion. [(a) : Satellite line, (b) : radiative line]

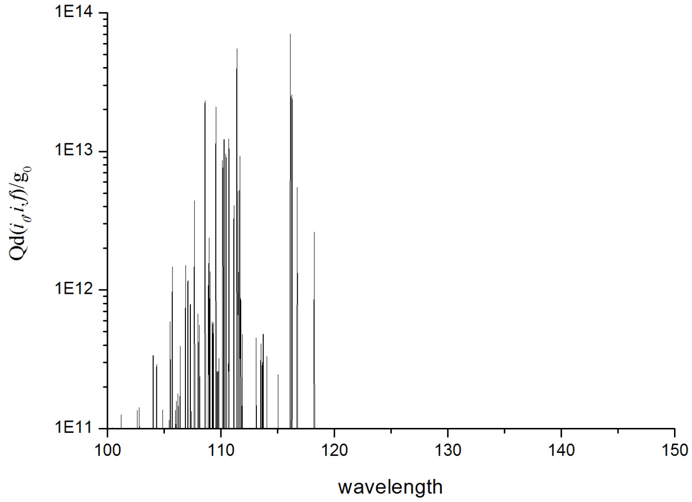

(a)

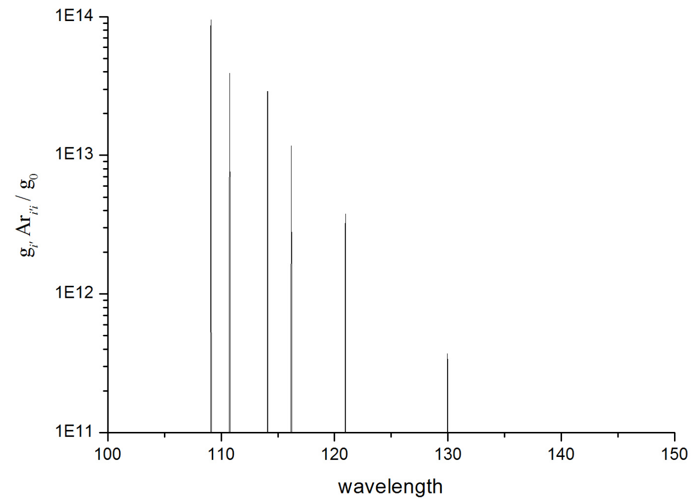

(b)

Figure 15: Satellite lines produced by dielectronic recombination ($4d^8\ ^3P_0 \rightarrow 4d^74f^2 \rightarrow 4d^84f^1$) of Xe^{9+} ion and radiative line that is obtained by radiative decay ($4d^74f^1 \rightarrow 4d^8\ ^3P_0$) of Xe^{10+} ion.[(a) : Satellite line, (b) : radiative line]

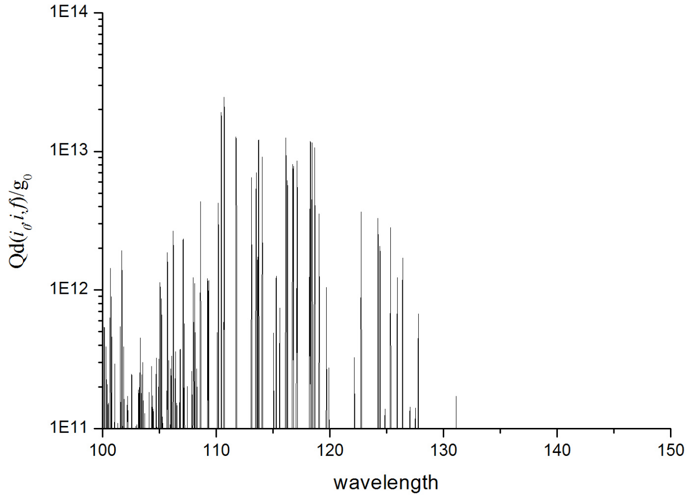

(a)

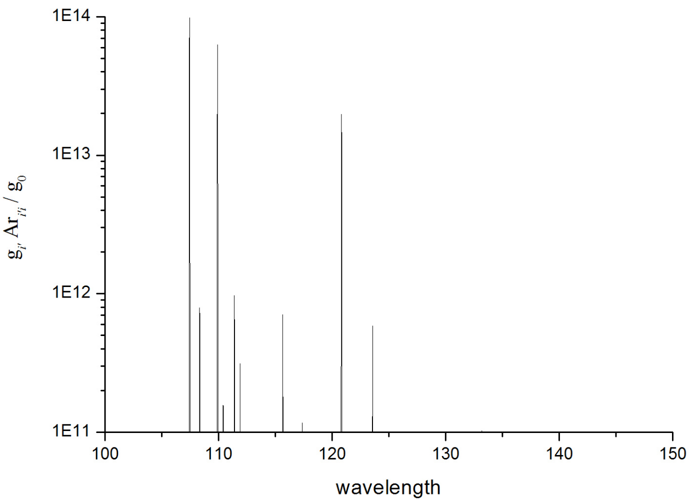

(b)

Figure 16: Satellite lines produced by dielectronic recombination ($4d^8\ ^1G_4 \rightarrow 4d^74f^2 \rightarrow 4d^84f^1$) of Xe^{9+} ion and radiative line that is obtained by radiative decay ($4d^74f^1 \rightarrow 4d^8\ ^1G_4$) of Xe^{10+} ion. [(a) : Satellite line, (b) : radiative line]

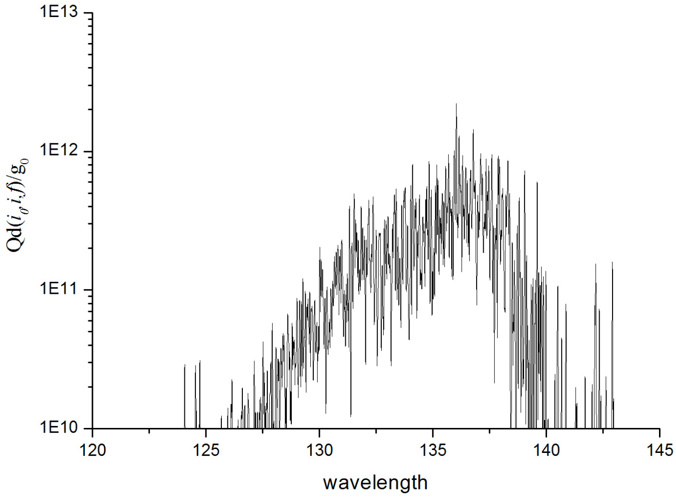

(a)

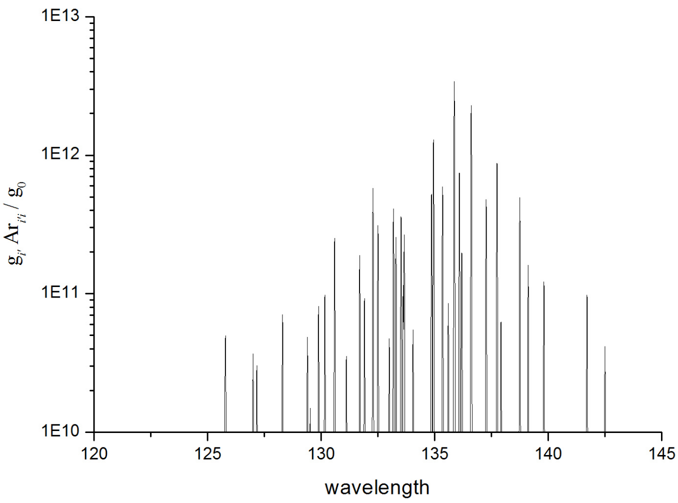

(b)

Figure 17: Satellite lines produced by dielectronic recombination ($4d^8\ ^3F_4 \rightarrow 4d^7 5p^1 5d^1 \rightarrow 4d^8 5d^1$) of Xe^{9+} ion and radiative line that is obtained by radiative decay ($4d^7 5p^1 \rightarrow 4d^8\ ^3F_4$) of Xe^{10+} ion. [(a) : Satellite line, (b) : radiative line]

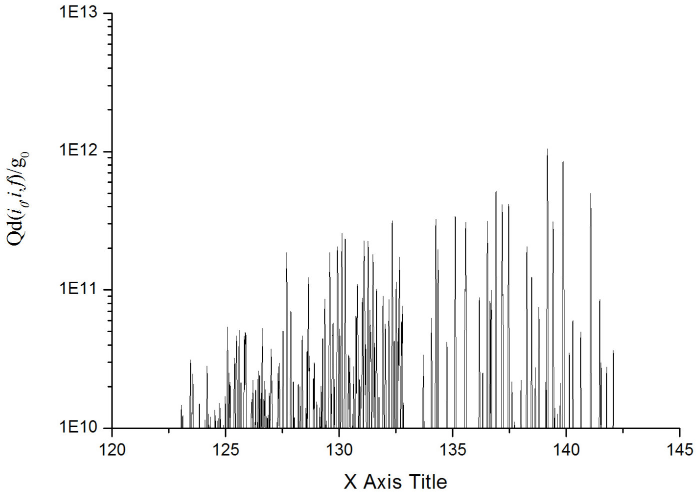

(a)

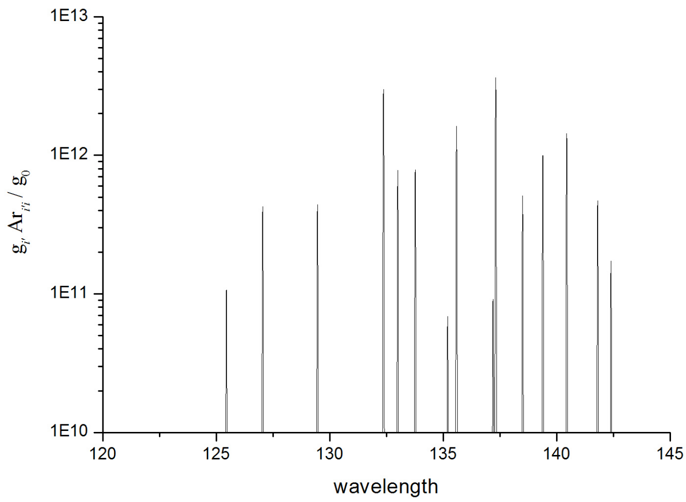

(b)

Figure 18: Satellite lines produced by dielectronic recombination ($4d^8\ ^3P_0 \rightarrow 4d^7 5p^1 5d^1 \rightarrow 4d^8 5d^1$) of Xe^{9+} ion and radiative line that is obtained by radiative decay ($4d^7 5p^1 \rightarrow 4d^8\ ^3P_0$) of Xe^{10+} ion.[(a) : Satellite line, (b) : radiative line]

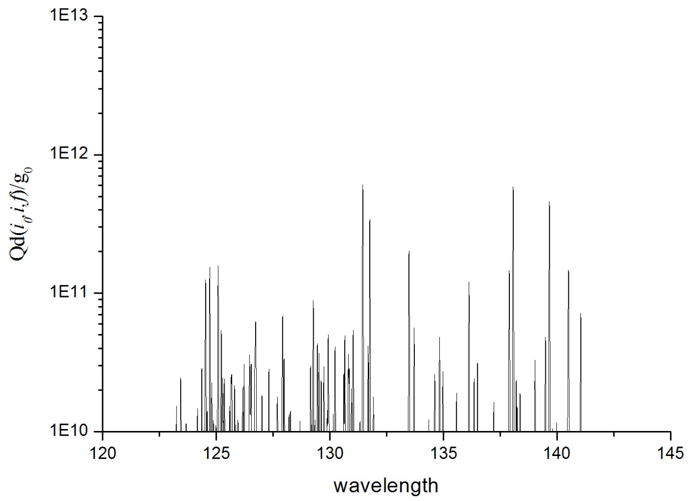

(a)

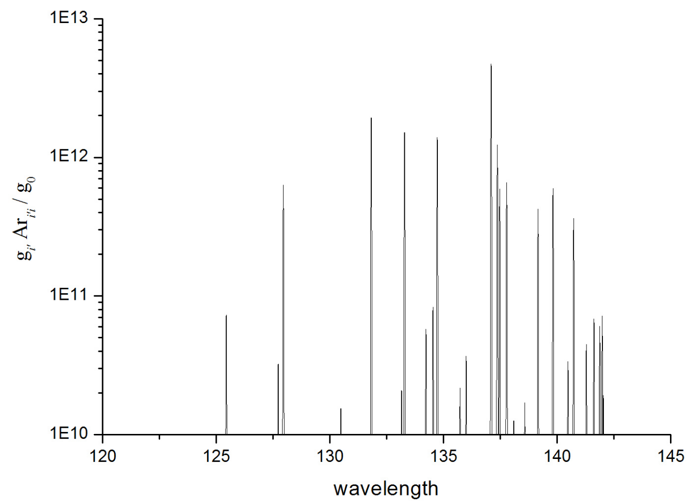

(b)

Figure 19: Satellite lines produced by dielectronic recombination ($4d^8\ ^1G_4 \rightarrow 4d^7 5p^1 5d^1 \rightarrow 4d^8 5d^1$) of Xe^{9+} ion and radiative line that is obtained by radiative decay ($4d^7 5p^1 \rightarrow 4d^8\ ^1G_4$) of Xe^{10+} ion. [(a) : Satellite line, (b) : radiative line]

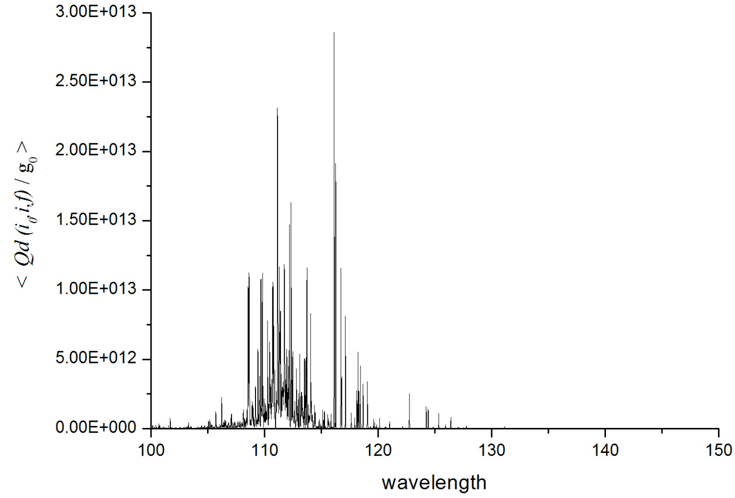

(a)

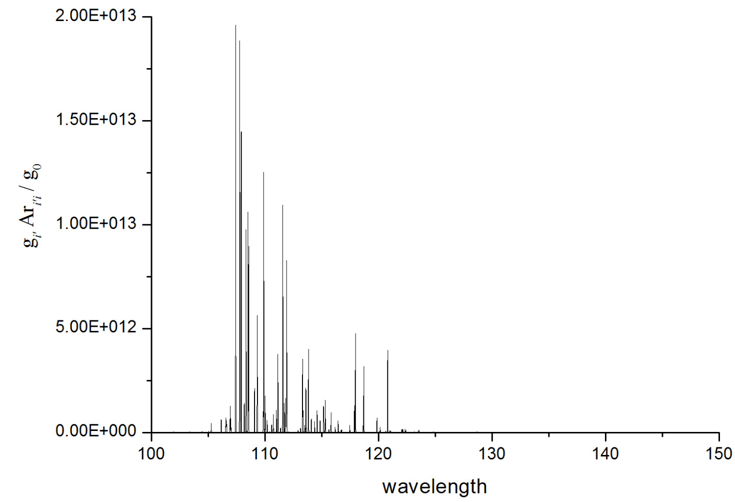

(b)

Figure 20: Satellite lines produced by dielectronic recombination ($4d^8 \rightarrow 4d^7 4f^2 \rightarrow 4d^8 4f^1$) of Xe^{9+} ion and radiative line that is obtained by radiative decay ($4d^7 4f^1 \rightarrow 4d^8$) of Xe^{10+} ion. [(a) : Satellite line, (b) : radiative line]

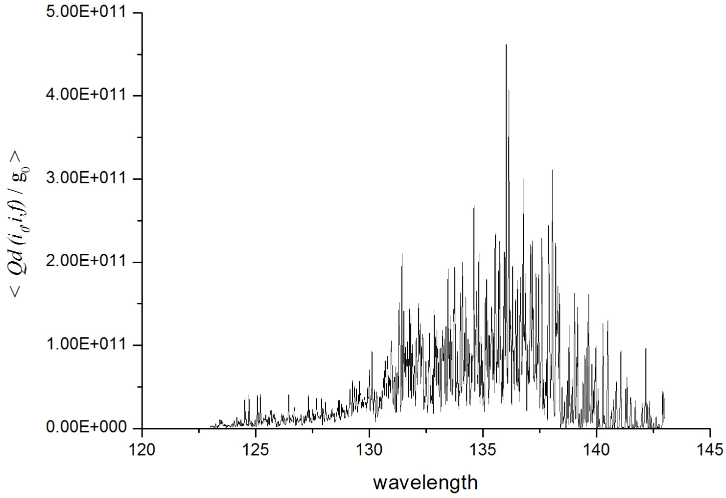

(a)

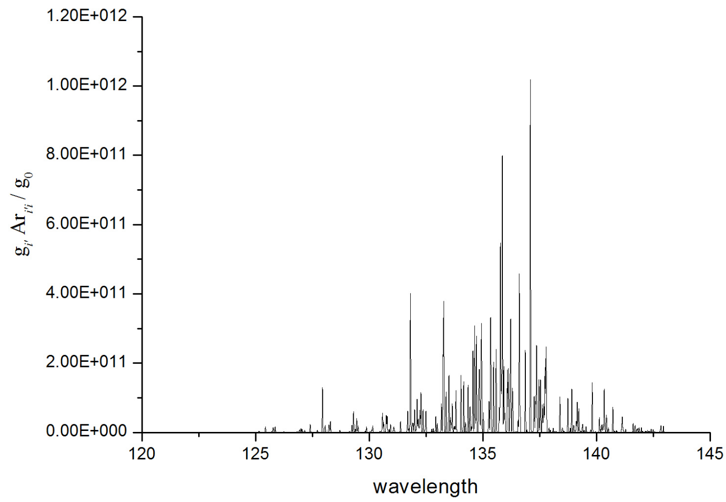

(b)

Figure 21: Satellite lines produced by dielectronic recombination ($4d^8 \rightarrow 4d^7 5p^1 5d^1 \rightarrow 4d^8 5d^1$) of Xe^{9+} ion and radiative line that is obtained by radiative decay ($4d^7 5p^1 \rightarrow 4d^8$) of Xe^{10+} ion. [(a) : Satellite line, (b) : radiative line]

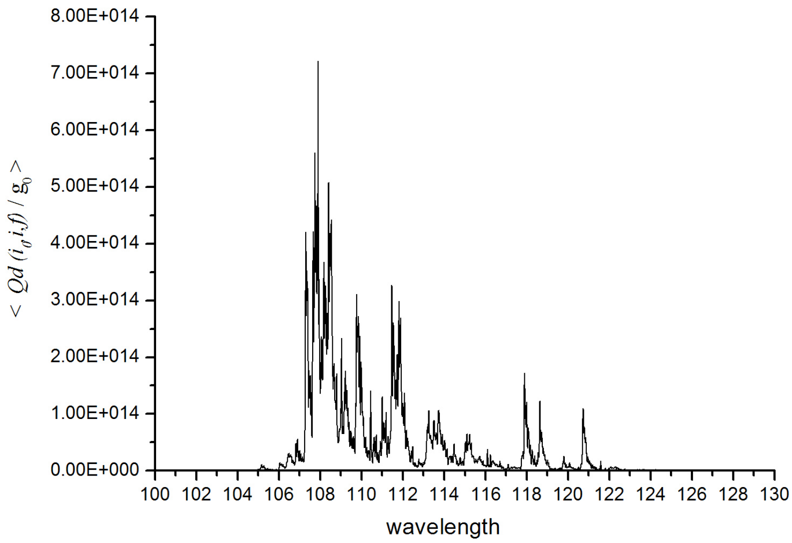

(a)

Figure 22: The satellite spectra for $\sum_{n=4}^{7} < Qd(4d^8, 4d^7 4f^1 nl, 4d^8 nl)/g_0 >$.

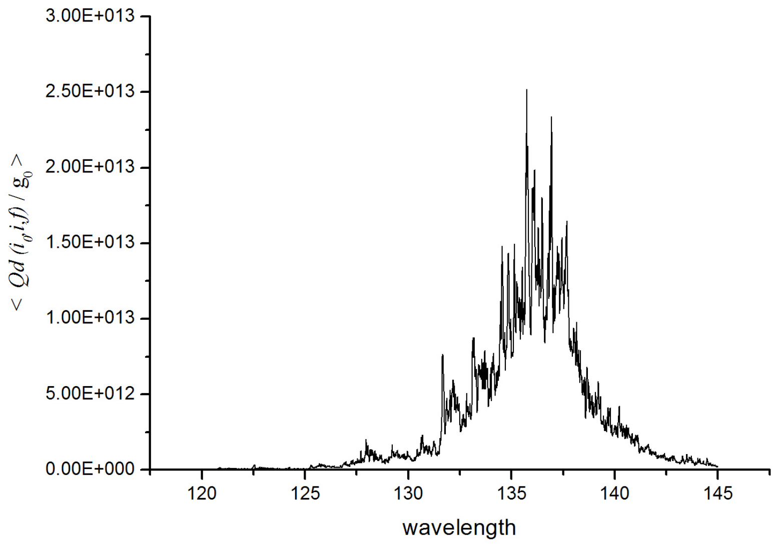

(a)

Figure 23: The satellite spectra for $\sum_{n=5}^{7} < Qd(4d^8, 4d^7 5p^1 nl, 4d^8 nl)/g_0 >$.

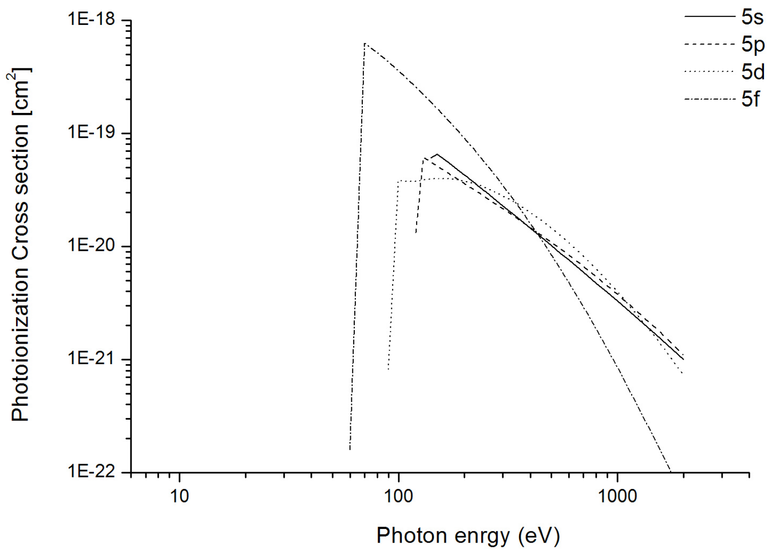

Figure 24: Photoionization cross section of Xe^{9+} ions calculated for different l with fixed $n = 5$.

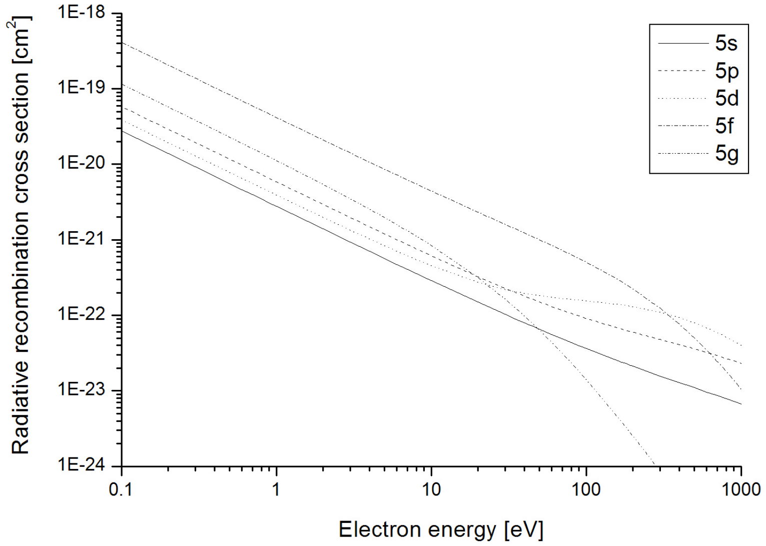

Figure 25: Radiative recombination cross section of Xe^{10+} ions calculated for different l with fixed $n = 5$.

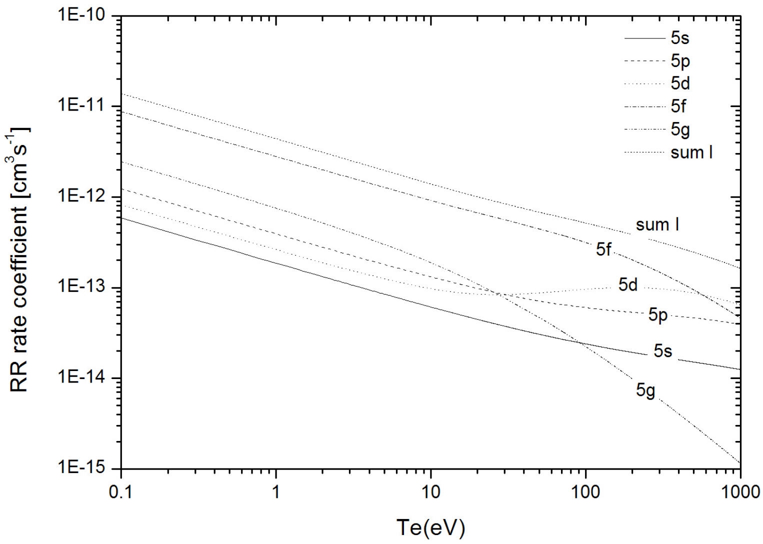

Figure 26: Radiative recombination rate coefficient of Xe^{10+} ions calculated for different l with fixed $n = 5$.

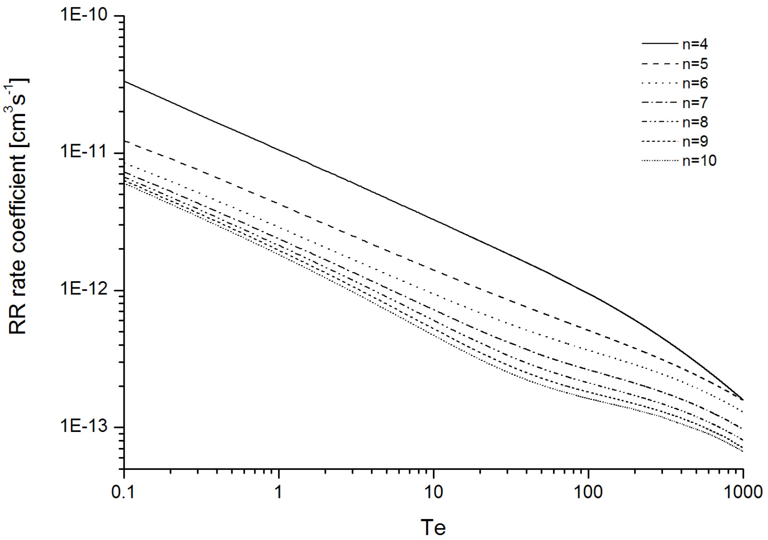

Figure 27: Radiative recombination rate coefficient of Xe^{10+} ions summed over all l but each different n as function of the electron temperature.

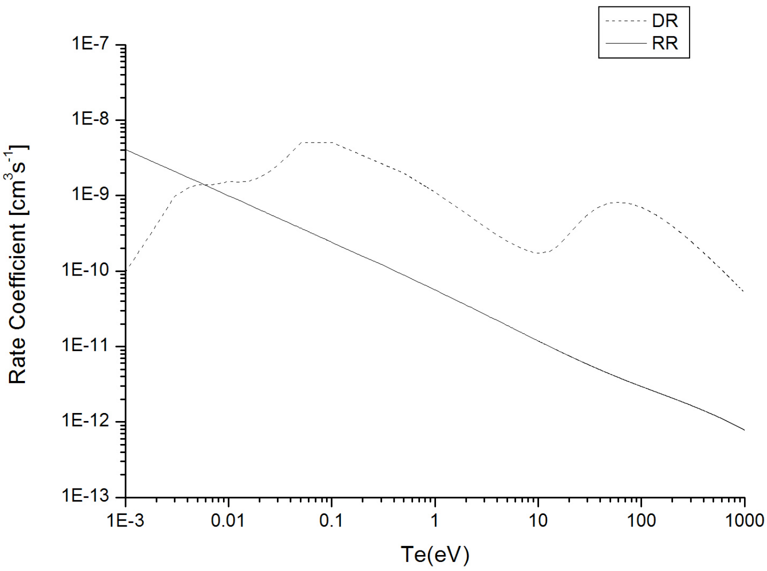

Figure 28: Comparison of total Dielectronic recombination rate coefficient for $4d^8 - 4d^7 4f^1 nl, 4d^7 5p^1 nl - 4d^8 nl$(solid line)[n = 4-100] and the radiative recombination rate coefficient for the $4d^8 \rightarrow 4d^8 nl$(dashed line) [n = 4-1000] of Xe^{10+} ions as function of the plasma temperature.